On Vortex Filament Methods for Linear Instability Analysis of Aircraft Wakes

Juan A. Tendero[a], Vassilios Theofilis[a], Miquel Roura[b], Rama Govindarajan[c]

[a] *School of Aeronautics, Universidad Politécnica de Madrid, Madrid, 28040, Spain*
[b] *Gamesa Innovation and Technology S.L., Madrid, 28043, Spain*
[c] *TIFR Centre for Interdisciplinary Sciences, Hyderabad, 500075, India*

Abstract

Linear stability analysis of vortical systems is discussed in a systematic manner using the classic inviscid vortex filament method. Well-known results are recovered as special cases of a unified linearization procedure. The symmetries of the vortex systems analyzed are exploited to obtain an analytical picture of different classes of growing and decaying eigenmodes. Finally, comparisons with viscous global linear theory reveal the limits of applicability of the vortex filament method for the instability analysis of realistic vortex systems.

Keywords: point vortex, vortex filament, aircraft wake, linear stability analysis

1. Introduction

The importance of understanding instability of trailing vortex systems has been highlighted in a number of sources, e.g. [1], and derives from the desire to minimize commercial aircraft separation distances, especially during take-off and landing. Indeed, the vortical wake of a large aircraft may impose a hazard for any following aircraft of similar size or smaller. It is precisely the lack of understanding of the actual mechanisms of vortex decay, especially in the near mid-field, which leads to potentially conservative choices being made by the regulating authorities as regards aircraft separation distances. Although the peak of activity surrounding the introduction of the Boeing 747 and the Airbus A380, in the 60's and 90's of last century respectively, has now subsided, the ever-increasing aircraft density in a finite size of air space [2] keeps providing motivation for studies aiming at quantifying aircraft wake destruction mechanisms.

In order to address aircraft wake instability, a particularly suitable analysis methodology is that based on modeling vortices as a set of vortex filaments. This inviscid modal linear stability theory was introduced by von Kármán [3, 4] and has been extremely useful in providing qualitative and on occasion quantitative information on linear flow dynamics of vortical systems. The vortex filaments theory has two variants: in its simplest form, introduced in the celebrated works of von Kármán [3, 4] and also denoted as *point vortex stability analysis*, the two-dimensional limit is considered. A vortical flowfield is reconstructed by a number of straight and parallel vortex filaments which can be viewed as (two-dimensional) point vortices in equilibrium, whose stability is analyzed. In an aeronautical context, Donaldson and Bilanin [5] have used this methodology to analyze different configurations of four aligned point vortices and assess whether placement of vortices of a given circulation at specific distances results in a system of vortices in equilibrium.

The second of the two variants mentioned before, is concerned to the three-dimensional limit. In reality, in this limit, the previous set of points are a set of straight and parallel vortex filaments. If motion of the vortex filament in the third spatial direction is permitted, one may introduce a sinusoidal perturbation to the position of the vortex filaments and study whether deviations from this position are amplified or damped. The seminal work of Crow [6] on a counter-rotating vortex pair exemplifies this *vortex filament instability analysis*. In that work, the so-called long-wavelength instability (now commonly known as *Crow instability*) of the wake was first predicted; the favorable comparison with experiments and observations lent strength to the underlying theoretical concept. Similar analysis

Email address: juanangel.tendero.ventanas@upm.es (Juan A. Tendero)

of Jiménez [7] for two vortices rotating in the same direction found this configuration to be stable, also in line with experimental observations. Many works followed, in which different initial vortex configurations are set, see e.g. Crouch [8], Rennich and Lele [9] and Fabre and Jacquin [10], among others.

Beyond the simplified configurations of two or more aligned filaments exposed previously, a wide variety of other vortical configurations have been analyzed with respect to their instability using the same methodology, such as the arrays of vortices situated at the vertices of a regular polygon, a configuration referred to as *n-gon*, originally studied by Kelvin [11] and Thomson [12]. Havelock [13] presented a consistent analysis of the same configuration, while half a century later, Campbell [14] reviewed the topic and added more results. However, it was not up until recent times that the $N = 7$ configuration was shown to be unstable by Kurakin and Yudovich [15]. An analogous configuration, the instability of which was first analyzed by Joukowski [16] using the vortex filament method, is the vortex n-gon to which an additional vortex is added at its center and is taken to rotate in the opposite sense as compared with the sense of rotation of the vortices of the n-gon. This model is the cornerstone of analyses of instabilities in the downwash of a helicopter rotor, as well as those in the wake behind wind turbines. Additional interesting examples of application of point-vortex or vortex-filament instability analysis include the three vortices discussed by Aref [17, 18], or other configurations involving a larger number of vortices [19]. Modifying the instability analysis methodology for straight vortex filaments, instability in a vortex helix can also be analyzed. This was first studied by Kelvin [20], and Levy and Forsdyke [21], while Ricca [22] and Kuibin and Okulov [23] added more light to the problem. Recently, instability in the wake of wind turbines was analyzed using an extension of the helical vortex filament method, in which multiple vortex helices with a common center are considered to model the tip vortices of the wind turbine blade, in the absence [24] or in the presence [25] of an additional counter-rotating vortex modeling the wake of the turbine nacelle.

While all the instability analysis methodologies briefly outlined above are inviscid in nature, viscous approaches are also numerous in the literature. Analysis of a single vortex by means of viscous local modal stability theory commenced by Lessen and Paillet [26] and continued in the works of Khorrami et al. [27], Khorrami [28, 29], and Mayer and Powell [30]. More recently viscous global modal stability analysis of the linearized Navier-Stokes equations [31, 32, 33], has also been applied to the instability of vortex systems [34, 35, 36, 37, 38, 39, 40]. Direct Numerical Simulations (DNS) and Large Eddy Simulations (LES) have been used to perform viscous instability analysis of vortical flows: Abid and Brachet [41] analyzed a single vortex, Laporte and Corjon [42] studied a vortex pair, Rennich and Lele [9] a four vortex wake, Bristol et al. [43] investigated a vortex pair of unequal strength, and Nybelen and Paoli [44] studied co-rotating vortices. Others analyze instabilities solving initial value problems (IVP) as it is done by means of DNS or LES, but based on the linearized Navier-Stokes equations (LNSE), as in the work of Billant et al. [45] for a particular vortex pair. In addition, DNS of vortex particles offers exceptionally good performance for vortical flows, particularly for wakes [46, 47, 48] and for helical vortices [49]. Last but not least, experiments focusing on the stability of vortical wake flows have provided key information on novel instability mechanisms of vortex systems: the works of Leweke and Williamson [50], Laporte and Leweke [51] and the review of Williamson [52] for the cylinder wake offer examples of the impact that experimentation on the instability of vortex flow systems has had on the understanding of vortex dynamics and instabilities. It is worth mentioning that 3D-DNS, LES and the experiments, despite the quality of results that they produce, may require expensive equipment or large computational resources and, as such, can be performed only for a limited number of parameters. By contrast inviscid linear modal stability analysis by vortex filaments can be solved analytically in most of the cases or computed using negligible computing resources and, as such, it is well suited to perform parametric studies of the different values of the variables involved in the instability problem.

After this demonstration of the enormous amount of works related to vortex instabilities, it is important to highlight that the present work is focused on linear instability. The reader might rightly think that the non-linear analysis will be more accurate, but it is also true that for understanding the non-linear behavior is usually needed to understand first the linear one. In addition, the linear analysis provides in general more information about how to actuate on these instabilities to control the system, as well as non-linear analysis is usually orders of magnitude more expensive in computational terms. The authors have then focused on linear analysis, provided also that there is more than sufficient material to be shown already. The non-linear study deserves its own analysis, and it is left for future work of these or other authors.

The present contribution begins with a systematic review of the inviscid modal linear stability analysis by vortex methods, highlighting the most relevant studies in each area. Some of the results shown here are new and complete

previous works, while some of the earlier results are reproduced in part here for consistency with the rest of the paper. The article is organized as follows. Section 2 discusses the theoretical concepts and deduces the equations solved, section 3 is devoted to the corresponding results, and finally, the summary, conclusions and closing comments are offered in section 4. Sections 2 and 3 are divided in three parts, one devoted to 2D inviscid analysis, another to its 3D counterpart and a third part is dedicated to the viscous theory and comparisons. The same scheme is followed both in the theoretical presentation and the results section. The two sections of inviscid theory (2D and 3D) begin with the theoretical concepts that lead to the general equations, which are subsequently made specific to a number of vortex configurations, starting from the most simple and advancing to the more complex.

2. Theory

The procedure carried out to perform the inviscid linear modal stability analysis by point vortices or vortex filaments is to obtain from the Biot-Savart law, the position derivatives (velocities) as function of the positions and intensities of all the vortices. These are then split into an equilibrium position and a small perturbation, and the equations are linearized. Additional assumptions can then be made, such as the selection of a homogeneous perturbation along the axial coordinate in the 3D case. The next step is to analyze the linear stability of the system by writing the time dependence as a complex exponential, and, obtain an eigenvalue problem for the complex frequencies. The values of these eigenvalues will determine the linear stability of the selected configuration of vortex filaments.

The inviscid vortex method for stability is based on idealized vortices that have an infinite value of vorticity concentrated at points or along filaments, and therefore, vortex size and vorticity distribution are not taken into account in this idealization. The importance of these effects is more relevant in the case of self-induction (the influence of one vortex over itself) and is negligible for the interactions among different filaments. This may seem to contradict the fact that the core size becomes more relevant when the vortices are closer, but the point is that in the equations (see Eqs. 17), the vortex size only affects the self induction term, and the proximity effect is noticeable only because first the self induction acts, and then, the close vortex amplifies the effect. Actually, that is true in the 3D case, while in the 2D case, there is no mention at all on vortex size, the point vortices are infinitely small, and the results are completely independent of vortex size. Therefore, only the 3D case will be affected by these features, as self-induction does not exist in the 2D case.

Consequently, in the point vortex stability analysis, the only relevant parameter of the vortices is their position, which will be the centroid of the real vortices. On the contrary, the integrals that appear in the 3D formulation may diverge and the analysis needs some modification to overcome this idealization. The simplest remedy is to use cutoff integrals, which consists in removing a small part from the integral in the process of integration. The length cut from the integral is what is called the *cutoff parameter*, or *cutoff length*, and its value will be a measure of the vortex size. Crow [6] suggested a proportionality relation between cutoff parameter and vortex radius, assuming that the filament is actually a Rankine vortex. Previously, Arms and Hama (see Hama [53] and Arms and Hama [54]) have already introduced the *localized-induction* concept, which is based on an expansion of the cutoff integral where the leading term is of order $\log(1/\varepsilon)$ being ε a small non-dimensional value proportional to the cutoff length. Several later works (Widnall et al. [55], Moore and Saffman [56], Widnall [57]) have exposed a more general relationship for different vortex core shapes, which even includes axial flow, by means of matching expansions between inner and outer velocity fields. Callegari and Ting [58], using the same methodology, obtained a formula for a vortex filament with viscous core, while Fukumoto and Miyazaki [59] extended the expansion to second order in the inviscid case, as well as Klein and Majda [60] derived a formula that includes self-stretching. The *localized-induction* concept, referred in more recent papers as local induction approximation (LIA), is the base of all the works mentioned above, and, additionally, is still leading to new developments as that from Segalini and Alfredsson [61], who derived a higher order formula for their particular case, a model of propeller/wind-turbine rotor wake. Most of these works, based on matching expansions, relate strictly the vortex core size and cutoff length, which couples the vortex core shape and the solution of the problem. In order to obtain more general results, this approach is not followed here, and the results are function of cutoff length instead of vortex core size. The choice of only using a cutoff, without an inner expansion matching, has an important disadvantage that the previous approaches that include an inner expansion do not have, which is that wavelengths shorter than the cutoff length cannot be analyzed, since they are removed. However, the results are independent of vortex core shape, and therefore more general for an unknown vortex shape. Only for comparison with other methodologies based in vortex size, the approach of Widnall [57] is chosen, where a

relationship between vortex core and cutoff length is given for a general vortex shape. Additional approaches could be used satisfactorily to study the short-wave instabilities as shown by Tsai and Widnall [62].

From the previous assumptions, core size and vortex shape are analyzed as a single parameter, the cutoff. Axial flow is another relevant feature for real flows that is not included in filament methods, although it could be taken as a further modification of the cutoff length. By definition, viscosity is not considered, and although there exist approaches permitting the addition of viscosity to time evolving vortex filament methods [46, 47, 49], application of viscous linear modal to stability analysis by vortex filaments is not straightforward. With these considerations in mind, it is now proceeded to derive the governing systems of equations both for the two dimensional and three dimensional cases, and, afterwards, the basics of viscous global modal stability analysis are exposed.

2.1. Two dimensional stability analysis

The linear stability of a set of point vortices is analyzed first, and the process of obtaining the matrix whose eigenvalues are sought in order to analyze the linear stability of the system is presented. The equations that establish the movement for a group of point vortices are obtained following the procedure discussed by Batchelor [63], in which the application of the vorticity definition, $\nabla \times \mathbf{u} = \boldsymbol{\omega}$, and the conditions of solenoidal incompressible fluid, $\nabla \cdot \boldsymbol{\omega} = 0$ and $\nabla \cdot \mathbf{u} = 0$, hold. In the case of study, the vorticity is concentrated in filaments, and it is zero in all the other parts of the domain. Then, the general form of the Biot-Savart law for vortex filaments is obtained:

$$\mathbf{u}(\mathbf{x}) = \frac{\Gamma}{4\pi} \int_L \frac{\mathrm{d}\mathbf{l}(\mathbf{x}') \times (\mathbf{x} - \mathbf{x}')}{\mid \mathbf{x} - \mathbf{x}' \mid^3}, \tag{1}$$

where $\mathrm{d}\mathbf{l} = \mathrm{d}s\, \boldsymbol{\omega} / \mid \boldsymbol{\omega} \mid$ is a vector tangent to the filament of vorticity and the circulation Γ can be extracted from the integral, because it is constant along the filament. This equation is written for the case of straight filaments in two spatial dimensions. For that, $\mathrm{d}\mathbf{l} = \mathbf{e_x}\mathrm{d}x'$, where x is chosen as the perpendicular direction to the plane. Note that $\mathbf{x}-\mathbf{x}' = -x'\mathbf{e_x} + (y-y')\mathbf{e_y} + (z-z')\mathbf{e_z}$ because the chosen plane is $x = 0$ for convenience. In general, this analysis should be performed for a configuration of N point vortices in a plane, the positions of which are given by $\mathbf{x}_p = [y_p, z_p]$, where the integer number p, and later also q, designate each point vortex. Therefore, the induced velocity is the sum for all of them, where one point cannot interact with itself and has been extracted from the addition:

$$\mathbf{u}(\mathbf{x}_p) = -\frac{1}{2\pi} \sum_{q=1,\, q\neq p}^{N} \Gamma_q \frac{(\mathbf{x}_p - \mathbf{x}_q) \times \mathbf{e_x}}{\mid \mathbf{x}_p - \mathbf{x}_q \mid^2} \tag{2}$$

The previous equation gives the velocity of the system of point vortices. However, the aim of this research is to study the stability of vortex systems. Before that, an equilibrium configuration of point vortices has to be chosen, which, introduced in Eq. (2), leads to $\mathbf{u}(\mathbf{x}_p) = 0$. Later in the next paragraph it will be encountered that this is not strictly true, and a system of vortices where the distances among them remain constant can be also chosen, and then, the velocities $\mathbf{u}(\mathbf{x}_p)$ can be different from zero, but equal for all the points. This equilibrium configuration, $\mathbf{X}_p = [Y_p, Z_p]$, is perturbed by $\mathbf{x'}_p = [y'_p, z'_p]$. Then, $\mathbf{x}_p = \mathbf{X}_p + \varepsilon \mathbf{x'}_p$[1] is substituted into Eq. (2) obtaining:

$$O(1): \quad \frac{\mathrm{d}\mathbf{X}_p}{\mathrm{d}t} + \bar{\mathbf{U}} = -\frac{1}{2\pi} \sum_{q=1,q\neq p}^{N} \Gamma_q \frac{\mathbf{X}_p - \mathbf{X}_q}{\mid \mathbf{X}_p - \mathbf{X}_q \mid^2} \times \mathbf{e_x} \tag{3a}$$

$$O(\varepsilon): \quad \frac{\mathrm{d}\mathbf{x'}_p}{\mathrm{d}t} = -\frac{1}{2\pi} \sum_{q=1,q\neq p}^{N} \Gamma_q \left(\frac{\mathbf{x'}_p - \mathbf{x'}_q}{\mid \mathbf{X}_p - \mathbf{X}_q \mid^2} - \frac{2(\mathbf{X}_p - \mathbf{X}_q) \cdot (\mathbf{x'}_p - \mathbf{x'}_q)}{\mid \mathbf{X}_p - \mathbf{X}_q \mid^4} (\mathbf{X}_p - \mathbf{X}_q) \right) \times \mathbf{e_x} \tag{3b}$$

$$O(\varepsilon^2): \quad \text{Neglected}, \tag{3c}$$

[1] Note that strictly speaking, $O(\varepsilon^2)$ and higher orders equations would imply constraints, but what it is done is a linearization, and therefore, higher order terms are neglected. However, to be more precise, it could be stated that $\mathbf{x}_p = \mathbf{X}_p + \varepsilon \mathbf{x'}_p + O(\varepsilon^2)$, and then everything is correct.

where the assumption $\varepsilon \ll 1$ is made. In the two dimensional case, $\mathbf{u}_p = [v_p, w_p] = \mathrm{d}\mathbf{x}_p/\mathrm{d}t = \mathbf{u}(\mathbf{x}_p) - \bar{\mathbf{U}}$, and therefore, $\mathbf{u}(\mathbf{x}_p) = \mathrm{d}\mathbf{x}_p/\mathrm{d}t + \bar{\mathbf{U}}$. The new term $\bar{\mathbf{U}}$ only appears when the basic state of the points is moving with constant speed, and it is necessary to change the reference system to one where the point vortices are stationary. Note that $\bar{\mathbf{U}}$ must be the same for all the vortices in order to have a reference system in which the set of points is in equilibrium.

The time derivative in Eq. (3a) vanishes when the initial points represent an equilibrium configuration. In fact, $\bar{\mathbf{U}}$ can be calculated from this equation. Eq. (3b) is the linearized equation of motion of the perturbations and will serve as the basis of the subsequent analysis. Eq. (3c) represents the neglected nonlinear terms.

Eq. (3b) is an Initial Value Problem (IVP) for the linearized equations, based upon which non-modal analysis could be performed, as done by Crouch [8]. In order to complete the modal analysis and obtain an EigenValue Problem (EVP), it is further assumed that the perturbation has a harmonic time variation that can be written in complex exponential form as $\mathbf{x'}_p = \hat{\mathbf{x}}_p \mathrm{e}^{-i\omega t}$. An EVP for ω results, in which stability can be inferred from the sign of the imaginary part of the eigenvalues. If $\omega_i > 0$, the perturbation grows and the mode is unstable, and if $\omega_i < 0$, the perturbation is damped and the mode is stable. $\omega_i = 0$ means that the mode is neutrally stable. On the other hand, ω_r is the frequency of oscillation of one particular mode in time. Explicitly, the EVP to solve in this case is:

$$-\mathrm{i}\omega\hat{y}_p = \sum_{q=1,q\neq p}^{N} \frac{-\Gamma_q}{2\pi}\left(\frac{\hat{z}_p - \hat{z}_q}{\zeta_{pq}^2} - \frac{2[\mathcal{Y}_{pq}(\hat{y}_p - \hat{y}_q) + \mathcal{Z}_{pq}(\hat{z}_p - \hat{z}_q)]\mathcal{Z}_{pq}}{\zeta_{pq}^4}\right) \tag{4a}$$

$$-\mathrm{i}\omega\hat{z}_p = \sum_{q=1,q\neq p}^{N} \frac{\Gamma_q}{2\pi}\left(\frac{\hat{y}_p - \hat{y}_q}{\zeta_{pq}^2} - \frac{2[\mathcal{Y}_{pq}(\hat{y}_p - \hat{y}_q) + \mathcal{Z}_{pq}(\hat{z}_p - \hat{z}_q)]\mathcal{Y}_{pq}}{\zeta_{pq}^4}\right) \tag{4b}$$

Eqs. (4) represent the general equations governing the stability of point vortices in Cartesian coordinates, where the variables $\mathcal{Y}_{pq} = Y_p - Y_q$, $\mathcal{Z}_{pq} = Z_p - Z_q$ and $\zeta_{pq} = \sqrt{(Y_p - Y_q)^2 + (Z_p - Z_q)^2}$ are introduced to simplify the notation. Along this procedure of calculations, the point vortices are assumed to be in equilibrium and perturbations to their original positions $(\hat{y}_p, \hat{z}_p)^T$ are always on the plane on which point vortices are defined. Points are regarded as infinite straight lines perpendicular to the plane.

Particular instability problems are solved by the introduction of appropriate values of the variables into Eqs. (4). In what follows, the configurations analyzed are taken to be of increasing complexity, starting with two vortices, counter-rotating as in Crow [6] or co-rotating as in Jiménez [7], then a particular configuration of four vortices that is steady, already studied by Rennich and Lele [9] and Fabre and Jacquin [10] and finally arrays of an infinite number of aligned vortices, initially studied by von Kármán [3, 4].

2.1.1. Two vortices

Two interesting cases of two point vortices exist, a counter-rotating and a co-rotating pair of vortices.

1. *Two counter-rotating vortices, Crow [6]*
   The eigenvalue problem is obtained substituting into Eqs. (4) the following: $N = 2$, $p = 1, 2$, $Y_1 = -b/2$, $Y_2 = b/2$, $Z_{1,2} = 0$, $\Gamma_1 = -\Gamma$ and $\Gamma_2 = \Gamma$, where b is the distance between the vortices and Γ is the circulation of the positive vortex, which makes the downwash between the vortices to move downwards. Note that the choice of these parameters derives from the existence of an equilibrium configuration in which $\bar{\mathbf{U}} = -(\Gamma/2\pi b)\mathbf{e_z}$ is the downwash speed of the vortex pair.
   The equations are written in non-dimensional form using the distance between the vortices as the characteristic length b, as well as the circulation of the right vortex as the characteristic circulation Γ. From that, the characteristic time scale is derived, $2\pi b^2/\Gamma$, which makes the non-dimensional downwash velocity unity. The values of the new non-dimensional variables are: $\tilde{\omega} = 2\pi\omega b^2/\Gamma$, $\tilde{y}_i = \hat{y}_i/b$ and $\tilde{z}_i = \hat{z}_i/b$. The system of equations can be written in the form of an eigenvalue problem, $-\mathrm{i}\tilde{\omega}\tilde{\mathbf{x}} = \mathbf{A}\tilde{\mathbf{x}}$:

$$-\mathrm{i}\tilde{\omega}\begin{pmatrix}\tilde{y}_1\\ \tilde{z}_1\\ \tilde{y}_2\\ \tilde{z}_2\end{pmatrix} = \begin{pmatrix}0 & -1 & 0 & +1\\ -1 & 0 & +1 & 0\\ 0 & -1 & 0 & +1\\ -1 & 0 & +1 & 0\end{pmatrix}\begin{pmatrix}\tilde{y}_1\\ \tilde{z}_1\\ \tilde{y}_2\\ \tilde{z}_2\end{pmatrix} \tag{5}$$

   The solution of this problem will be presented in section 3.1.1.

2. *Two co-rotating vortices, Jiménez [7]*
The only difference with the case of counter-rotating vortices is the change of sign in the circulation of one vortex. When that is done, it is found that $\bar{\mathbf{U}} = \pm(\Gamma/2\pi b)\mathbf{e_z}$, for the vortex 2 and 1 respectively, which are not the same, and therefore, the configuration is not in equilibrium in that reference frame. In order to overcome this difficulty, Jiménez [7] chose a rotating reference system, where x is a common coordinate for both vortices, y is the radial coordinate, pointing outward, and z is the azimuthal coordinate following the direction of the movement of each vortex. Eqs. (4) are re-written changing the sign of $\hat{y}_2$ and $\hat{z}_2$ and taking for the vortex 1, $Y_1 = 0$, $Y_2 = -b$ and for the vortex 2, $Y_1 = -b$, $Y_2 = 0$, all the rest remaining equal. Using that system, $\bar{\mathbf{U}} = (\Gamma/2\pi b)\mathbf{e_z}$ becomes the same for the two vortices. Furthermore, as the reference system is rotating, a new term appears, as $[\mathrm{d}\mathbf{x'}_p/\mathrm{d}t]_{\text{Inertial}} = [\mathrm{d}\mathbf{x'}_p/\mathrm{d}t]_{\text{rotating}} + \mathbf{\Omega} \times \mathbf{x'}_p$, where $\mathbf{\Omega} = \Gamma/(\pi b^2)\mathbf{e_x}$ is the angular velocity. The non-dimensionalization could have been done choosing πb as distance and Γ as circulation. Time would then be non-dimensionalized by $2\pi^2 b^2/\Gamma$, which is the time needed to propagate a distance πb, that is one turn. However, that will lead to a single multiplicative constant π in the equations. For this reason the same non-dimensionalization is used here as for the case of the counter-rotating vortices. The values of the new variables are again: $\tilde{\omega} = 2\pi\omega b^2/\Gamma$, $\tilde{y}_i = \hat{y}_i/b$ and $\tilde{z}_i = \hat{z}_i/b$. The system of equations is written in the form of an eigenvalue problem, which will also be solved in section 3.1.1.

$$-\mathrm{i}\tilde{\omega}\begin{pmatrix}\tilde{y}_1\\ \tilde{z}_1\\ \tilde{y}_2\\ \tilde{z}_2\end{pmatrix} = \begin{pmatrix}0 & 1 & 0 & -1\\ -3 & 0 & -1 & 0\\ 0 & -1 & 0 & 1\\ -1 & 0 & -3 & 0\end{pmatrix}\begin{pmatrix}\tilde{y}_1\\ \tilde{z}_1\\ \tilde{y}_2\\ \tilde{z}_2\end{pmatrix} \tag{6}$$

2.1.2. Four aligned vortices, Rennich and Lele [9] and Fabre and Jacquin [10]

Configurations of two aligned vortex pairs with a common center of symmetry are analyzed in this section. The values for the parameters appearing in Eqs. (4) that define these configurations are: $N = 4$, $Z_1 = Z_2 = Z_3 = Z_4 = 0$, $Y_1 = -Y_4$, $Y_2 = -Y_3$, $\Gamma_1 = -\Gamma_4$ and $\Gamma_2 = -\Gamma_3$. This set of values does not necessarily lead to an equilibrium configuration, and different situations can occur. The configuration may diverge, it may have a periodic movement or it may be stationary, that is, the vortices will move together keeping the same distances among them. Donaldson and Bilanin [5] first studied these different situations, and Fabre et al. [64] showed the different regions in a more clear way. Only the equilibrium configuration is studied here, which is obtained when $\bar{\mathbf{U}}$ is imposed to be the same for all four vortices. In fact, due to the symmetry of the problem, this condition only needs to be imposed to the inner and outer vortices on one side. Eq. (3a) is used for that purpose, which leads to the celebrated cubic equation first derived by Rennich and Lele [9], (see also Jacquin et al. [36]):

$$\mathcal{X}^3 + 3\mathcal{G}\mathcal{X}^2 + 3\mathcal{X} + \mathcal{G} = 0, \tag{7}$$

where $\mathcal{X} = Y_3/Y_4$ and $\mathcal{G} = \Gamma_3/\Gamma_4$. The implication is that any ratio between circulations, $\mathcal{G}$, will lead to a ratio between inner and outer vortex positions. If the equation is written as $\mathcal{G}(\mathcal{X}) = -\mathcal{X}(\mathcal{X}^2 + 3)/(3\mathcal{X}^2 + 1)$, the following properties are deduced: $\mathcal{G}(-\mathcal{X}) = -\mathcal{G}(\mathcal{X})$ and $\mathcal{G}(1/\mathcal{X}) = 1/\mathcal{G}(\mathcal{X})$. Therefore, as the solution is odd, negative values of $\mathcal{X}$ do not offer additional results to these obtained by the positive values, and, due to the second property, results for $|\mathcal{X}| > 1$ are already considered when $1/|\mathcal{X}| < 1$ is analyzed. Therefore, only the range $0 < \mathcal{X} < 1$ and $-1 < \mathcal{G} < 0$ is considered because it includes all the possible solutions. Fig. 1 shows the solution of Eq. (7) for that range.

With the understanding that $\mathcal{X}$ is a function of $\mathcal{G}$, the parameters appearing in Eqs. (4) take the values: $N = 4$, $Z_1 = Z_2 = Z_3 = Z_4 = 0$, $Y_1 = -b_1/2$, $Y_2 = -b_2/2 = -\mathcal{X}b_1/2$, $Y_3 = b_2/2 = \mathcal{X}b_1/2$, $Y_4 = b_1/2$, $\Gamma_1 = -\Gamma_0$, $\Gamma_2 = -\mathcal{G}\Gamma_0$, $\Gamma_3 = \mathcal{G}\Gamma_0$, $\Gamma_4 = \Gamma_0$, where b_1 and b_2 are the distances between the outer and the inner vortices respectively. Substituting these parameters into Eqs. (4) and non-dimensionalizing all variables, an EVP $-\mathrm{i}\tilde{\omega}\tilde{\mathbf{x}} = \mathbf{A}\tilde{\mathbf{x}}$ results:

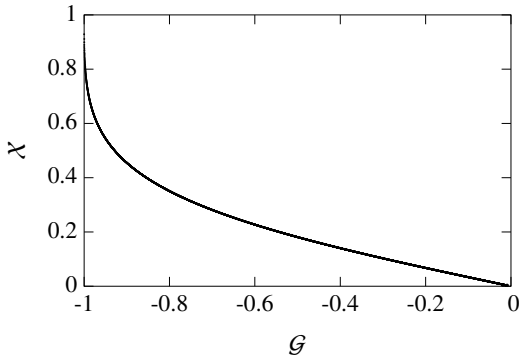

Figure 1: Solution of the equation of equilibrium for four point vortices.

$$-\mathrm{i}\tilde{\omega}\begin{pmatrix}\tilde{y}_1\\ \tilde{z}_1\\ \tilde{y}_2\\ \tilde{z}_2\\ \tilde{y}_3\\ \tilde{z}_3\\ \tilde{y}_4\\ \tilde{z}_4\end{pmatrix} = \begin{pmatrix} 0 & G_5 & 0 & \mathcal{G}G_2 & 0 & -\mathcal{G}G_1 & 0 & -G_3\\ G_5 & 0 & \mathcal{G}G_2 & 0 & -\mathcal{G}G_1 & 0 & -G_3 & 0\\ 0 & G_2 & 0 & G_6 & 0 & -\mathcal{G}G_4 & 0 & -G_1\\ G_2 & 0 & G_6 & 0 & -\mathcal{G}G_4 & 0 & -G_1 & 0\\ 0 & G_1 & 0 & \mathcal{G}G_4 & 0 & -G_6 & 0 & -G_2\\ G_1 & 0 & \mathcal{G}G_4 & 0 & -G_6 & 0 & -G_2 & 0\\ 0 & G_3 & 0 & \mathcal{G}G_1 & 0 & -\mathcal{G}G_2 & 0 & -G_5\\ G_3 & 0 & \mathcal{G}G_1 & 0 & -\mathcal{G}G_2 & 0 & -G_5 & 0 \end{pmatrix}\begin{pmatrix}\tilde{y}_1\\ \tilde{z}_1\\ \tilde{y}_2\\ \tilde{z}_2\\ \tilde{y}_3\\ \tilde{z}_3\\ \tilde{y}_4\\ \tilde{z}_4\end{pmatrix} \tag{8}$$

The eigenvalues $\tilde{\omega}$ of the matrix **A** provide the stability of the system. The distances are non-dimensionalized by the distance between the centroids of each side pair of vortices b and the circulation by the sum of the two different circulations Γ, as done by Crouch [8]. The characteristic time is then $2\pi b^2/\Gamma$. $\Gamma = (1+\mathcal{G})\Gamma_0$, $b = (1+\mathcal{X}\mathcal{G})b_1/(1+\mathcal{G})$, $\tilde{\omega} = 2\pi\omega b^2/\Gamma$, $\tilde{y}_i = \hat{y}_i/b$ and $\tilde{z}_i = \hat{z}_i/b$ are the values that have been used in order to obtain G_i of Eqs. (8), which are given in Eqs. (9).

$$\begin{aligned} G_1 &= \frac{4(1+\mathcal{X}\mathcal{G})^2}{(1+\mathcal{G})^3(1+\mathcal{X})^2} & G_2 &= \frac{4(1+\mathcal{X}\mathcal{G})^2}{(1+\mathcal{G})^3(1-\mathcal{X})^2}\\ G_3 &= \frac{(1+\mathcal{X}\mathcal{G})^2}{(1+\mathcal{G})^3} & G_4 &= \frac{(1+\mathcal{X}\mathcal{G})^2}{(1+\mathcal{G})^3\mathcal{X}^2}\\ G_5 &= \mathcal{G}(G_1-G_2)+G_3 & G_6 &= G_1-G_2+\mathcal{G}G_4 \end{aligned} \tag{9}$$

2.1.3. Infinite row of vortices, von Kármán [3, 4]

In the previous examples, wakes are considered in which the axis of the vortices is the same as the direction of motion of the aircraft whose wake is modeled. By contrast, in a two dimensional profile or bluff body, the wake can be seen as an infinite arrangement of aligned vortices downstream the body and its stability may be analyzed following the seminal works of von Kármán [3, 4]. In all cases studied in this section, an additional step has to be made due to the infinite number of point vortices considered. A sinusoidal perturbation of periodicity φ times the separation between consecutive vortices is imposed. This assumption allows to reproduce a wide number of different modes of perturbations corresponding to finite values of a single parameter, φ. This parameter is taken to be continuous, $0 \leq \varphi < 2\pi$, since higher values mean that the periodicity length is smaller than the distance between points. The meaning of parameter φ is that it fixes the number of point vortices needed to repeat periodicity as $N = 2\pi/\varphi$, and therefore, although it could be taken from the continuous, it is usually better to select the number of points N and calculate the corresponding value of the parameter φ. Doing that, for each value of the parameter φ, the number of degrees of freedom is equal to twice the number of different points considered.

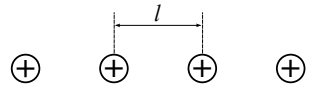

(a) Equidistant aligned vortices rotating in the same sense.

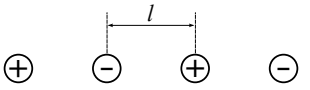

(b) Equidistant aligned vortices rotating in alternating senses.

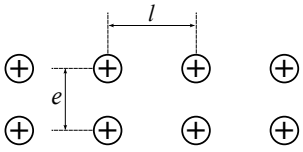

(c) Two rows of equidistant aligned vortices rotating in the same sense, one on top of the other.

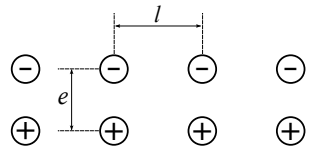

(d) Two rows of equidistant aligned vortices rotating in opposite senses, one on top of the other.

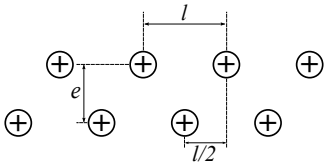

(e) Two rows of equidistant aligned vortices rotating in the same sense, displaced half distance.

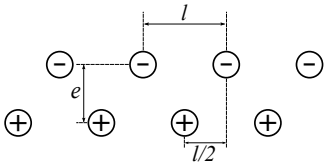

(f) Two rows of equidistant aligned vortices rotating in opposite senses, displaced half distance.

Figure 2: Vortex location scheme for various configurations of infinite number of vortices.

1. *Equidistant aligned vortices rotating in the same sense*
   This is the most simple configuration of this kind, shown in Fig. 2(a), and is composed of an infinite set of equidistant aligned vortices of the same strength and direction of rotation. This configuration is an idealization of a vortex sheet, that appears in the interface of two regions of different speeds.
   In all cases, the number of different points to be considered in the analysis first needs to be identified. All the points are equal here, so only one point vortex needs to be considered, named point 0.
   Second, the condition needs to be derived for the system to remain in equilibrium. For that, Eq. (3a) is written for a single point $p = 0$. $Z_q = 0$ and $Y_q = ql$, in particular, $Z_0 = 0$ and $Y_0 = 0$. l is the distance between vortices, $-\infty < q < \infty$ and $\Gamma_q = \Gamma$ for every q. Remember that both p and q are integers as they define different point vortices. In this case $\bar{\mathbf{U}} = 0$ and the configuration is in equilibrium.
   The stability analysis is performed using Eqs. (4) for the point $p = 0$. Next, a sinusoidal perturbation of the form $(\hat{y}_q, \hat{z}_q)^T = (\hat{y}_0, \hat{z}_0)^T \mathrm{e}^{qi\varphi}$ is imposed, which results in:

$$-\mathrm{i}\omega\hat{y}_0 = -\frac{\Gamma\hat{z}_0}{\pi l^2}\sum_{q=1}^{\infty}\frac{1-\cos(q\varphi)}{q^2} \tag{10a}$$

$$-\mathrm{i}\omega\hat{z}_0 = -\frac{\Gamma\hat{y}_0}{\pi l^2}\sum_{q=1}^{\infty}\frac{1-\cos(q\varphi)}{q^2} \tag{10b}$$

   From now on, the positive real function of the parameter φ, $f_1(\varphi)$ is considered[2]. If the distance is non-dimensionalized by l and ω by $\Gamma/\pi l^2$, the problem can be written in matrix form as an EVP, for the non-dimensional perturbations to the position vector $(\tilde{y}_0, \tilde{z}_0) = (\hat{y}_0, \hat{z}_0)/l$ and the eigenvalues $\tilde{\omega} = \pi l^2\omega/\Gamma$.

$$-\mathrm{i}\tilde{\omega}\begin{pmatrix}\tilde{y}_0\\ \tilde{z}_0\end{pmatrix} = \begin{pmatrix}0 & -f_1(\varphi)\\ -f_1(\varphi) & 0\end{pmatrix}\begin{pmatrix}\tilde{y}_0\\ \tilde{z}_0\end{pmatrix} \tag{11}$$

[2]This and subsequent formulas are collected in Appendix A

2. *Equidistant aligned vortices rotating in alternating senses*
   This configuration is seen in Fig. 2(b). The full process is similar to the previous case, only that the sign of the vortices has to be changed alternately. Again the vortices are in equilibrium as $\bar{\mathbf{U}} = 0$ and due to the alternation of the sign of the vortices, a new function $f_2(\varphi)$ appears, which is a negative real function of the parameter φ.

$$-\mathrm{i}\tilde{\omega}\begin{pmatrix} \tilde{y}_0 \\ \tilde{z}_0 \end{pmatrix} = \begin{pmatrix} 0 & -f_2(\varphi) \\ -f_2(\varphi) & 0 \end{pmatrix}\begin{pmatrix} \tilde{y}_0 \\ \tilde{z}_0 \end{pmatrix} \tag{12}$$

3. *Two rows of equidistant aligned vortices rotating in the same sense, one on top of the other*
   The configuration analyzed here is shown in Fig. 2(c), and consists of two lines of vortices, all rotating in the same sense, where the vortices coincide one on top of the other. In contrast to the previous cases, there exist two different kind of points, one corresponding to the upper row, denoted as 0^+, and one to the lower, denoted as 0^-.
   As before, the first concern is to ensure that the configuration is in equilibrium. That is inquired by solving Eq. (3a) for the two points, $p = 0^+, 0^-$. The respective locations are $Z_{q^+} = e$, $Z_{q^-} = 0$, $Y_q = ql$, where e is the distance between the rows and l is the distance between points. For this configuration, there are two sums of q, one for the upper row, and another for the lower row. The circulations are the same, $\Gamma_q = \Gamma$, for all q.
   The result is that $\bar{U}_z = 0$, but $\bar{U}_y = \pm\Gamma f_3(l/e)/(2\pi e)$ (negative for the upper row and positive for the lower), where $f_3(l/e)$ is a real positive function of the ratio between horizontal and vertical spacing, higher than one and tending to infinity as $l/e \to 0$. $f_3(l/e)$ is written in series form in Appendix A, but it has an analytic form: $f_3(l/e) = \pi/(l/e)\mathrm{Coth}[\pi/(l/e)]$. Therefore, $\bar{U}_y$ is different for the two rows, the upper moves to the left, while the lower does it to the right and the system is not in equilibrium. In other words, the stability question cannot be addressed for this configuration, since the system is not in equilibrium.
4. *Two rows of equidistant aligned vortices rotating in opposite senses, one on top of the other, von Kármán [4]*
   This configuration, shown in Fig. 2(d), is analogous with that of the previous case, but now, the point vortices of the upper and lower rows rotate in opposite senses. Without loss of generality, the lower row is taken to have positive circulation and negative the upper. The values of the problem parameters are: $p = 0^+, 0^-$, $Z_{q^+} = e$, $Z_{q^-} = 0$, $Y_q = ql$, $\Gamma_{q^+} = -\Gamma$ and $\Gamma_{q^-} = \Gamma$.
   In contrast with the previous case, this time a reference system in which the two rows are in equilibrium does exist. The system is that moving with the vortices to the left with the velocity $\bar{U}_y = -\Gamma f_3(l/e)/(2\pi e)$, while $\bar{U}_z = 0$, as expected. Therefore, the stability analysis can be performed using Eqs. (4) for two points, one from the upper row ($p = 0^+$) and other from the lower row ($p = 0^-$). A sinusoidal perturbation of the form $(\hat{y}_{q^\pm}, \hat{z}_{q^\pm})^T = (\hat{y}_{0^\pm}, \hat{z}_{0^\pm})^T \mathrm{e}^{q\mathrm{i}\varphi}$ is again imposed.
   The real functions $f_4(l/e)$ (positive and lower than 1), $f_5(\varphi, l/e)$ and $f_6(\varphi, l/e)$ (both positive or negative for different values of φ and l/e, and their absolute value always lower than unity) are defined in order to simplify the presentation. The problem is also non-dimensionalized, and the notation is further simplified. As originally done by von Kármán [4], new functions are introduced: $A_1(\varphi, l/e)$ and $C_1(\varphi, l/e)$ real and $B_1(\varphi, l/e)$ imaginary. In the notation introduced, the eigenvalue problem can now be stated:

$$-\mathrm{i}\tilde{\omega}\begin{pmatrix} \tilde{y}_{0^+} \\ \tilde{z}_{0^+} \\ \tilde{y}_{0^-} \\ \tilde{z}_{0^-} \end{pmatrix} = \begin{pmatrix} 0 & A_1 & B_1 & -C_1 \\ A_1 & 0 & -C_1 & -B_1 \\ B_1 & C_1 & 0 & -A_1 \\ C_1 & -B_1 & -A_1 & 0 \end{pmatrix}\begin{pmatrix} \tilde{y}_{0^+} \\ \tilde{z}_{0^+} \\ \tilde{y}_{0^-} \\ \tilde{z}_{0^-} \end{pmatrix}, \tag{13}$$

   as first formulated by von Kármán [4]
5. *Two rows of equidistant aligned vortices rotating in the same sense, displaced half distance*
   The configuration of two rows of equidistant aligned vortices rotating in the same sense, one on top of the other is now displaced a distance that is half of the spacing between vortices of the same row in a staggered pattern shown in Fig. 2(e).
   As before, there exist two different kind of points, the upper row (0^+) and the lower row (0^-). The point locations are $Z_{q^+} = e$, $Z_{q^-} = 0$, $Y_{q^+} = q^+ l$ and $Y_{q^-} = (q^- - sign(q^-)/2)l$. The circulations are all the same, $\Gamma_q = \Gamma$ for all q.

The result is the same as obtained in case 3 of this chapter, although function $f_3(l/e)/2$ is changed in this case by $f_7(l/e)$. This is a positive real function of a qualitative shape similar to $1/x$, being unbounded for $l/e \to 0$ and 0 when $l/e \to \infty$. The series form of $f_7(l/e)$ is collected in Appendix A, but in this case again, an analytic form exists: $f_7(l/e) = i(\psi[1/2 - i/(l/e)] - \psi[1/2 + i/(l/e)])/(2l/e)$, being $\psi(x)$ ~~is~~ the digamma function [65]. That is, $\bar{U}_z = 0$ and $\bar{U}_y = \pm\Gamma f_7(l/e)/(\pi e)$, and again, the upper row moves to the left and the lower to the right. As in the earlier case 3, this configuration is not in equilibrium and no stability analysis may be performed.

6. *Two rows of equidistant aligned vortices rotating in opposite senses, displaced half distance, von Kármán [4]*
The last configuration of infinite rows analyzed is shown in Fig. 2(f). It is analogous with that in the previous case, but the point vortices of the upper and lower rows rotate in opposite senses. The particular parameters of the problem are: $p = 0^+, 0^-$, $Z_{q^+} = e$, $Z_{q^-} = 0$, $Y_{q^+} = q^+ l$ and $Y_{q^-} = (q^- - sign(q^-)/2)l$, $\Gamma_{q^+} = -\Gamma$ and $\Gamma_{q^-} = \Gamma$. This configuration led to the celebrated work of von Kármán [4], which describes the topology of a wake bearing his name, and provides the best point-vortex approximation of the wake of a bluff body.
The procedure to follow is the same as in the earlier cases, the only difference being the displacement of the vortices. Again, $\bar{U}_z = 0$, and the system moves with constant horizontal speed $\bar{U}_y = -\Gamma f_7(l/e)/(\pi e)$, which can be computed analytically.
In addition, new real functions are defined: $f_8(l/e)$, always positive and small, $f_9(\varphi, l/e)$, taking positive or negative values and $f_{10}(\varphi, l/e)$, also taking positive or negative values. These functions are used to define $A_2(\varphi, l/e)$, real, $B_2(\varphi, l/e)$ imaginary, and $C_2(\varphi, l/e)$, real. Using these new functions, the problem follows the same equations as Eqs. (13), where subindex 1 is changed by 2. Therefore, the relations between A_1, B_1 and C_1, can be directly applied here to A_2, B_2 and C_2.

2.2. Three dimensional stability analysis

The approach followed in this section is analogous to that adopted in the two dimensional case, but now, the previously considered straight parallel filaments can have homogeneous perturbations along the perpendicular x direction. The equation that governs the movement of each of the filaments is Eq. (1), which, extended to a number N of filaments results into the following equation:

$$\mathbf{u}(\mathbf{x}_p) = -\frac{1}{4\pi}\sum_{q=1}^{N}\Gamma_q \int_L \frac{(\mathbf{x}_p - \mathbf{x}_q)\times \mathrm{d}\mathbf{l}_q}{|\,\mathbf{x}_p - \mathbf{x}_q\,|^3} \tag{14}$$

An important particularity of Eq. (14) is self-induction, namely that one filament can interact with itself, and therefore, the constraint $p \neq q$ has been removed. However, as mentioned earlier, these integrals diverge and cutoff integrals are used, as originally suggested by Crow [6].

As regards modal linear stability analysis, a similar procedure to that followed in the two dimensional case is carried out to obtain the matrix whose eigenvalues are sought. The positions of the vortices ($\mathbf{x}_p = [x_p, y_p, z_p]$) are decomposed into a basic state ($\mathbf{X}_p = [X_p, Y_p, Z_p]$) and a perturbation ($\mathbf{x'}_p = [0, y'_p, z'_p]$) of order $\varepsilon \ll 1$[3]. This time, $\mathrm{d}\mathbf{l}_q = (\partial\mathbf{x}_q/\partial x_q)\mathrm{d}x_q = (\mathbf{e_x} + \varepsilon\partial\mathbf{x}'_q/\partial x_q)\mathrm{d}x_q$ as the filaments are now perturbed. Perturbations are only supposed to act in the perpendicular plane, while the x coordinate is only an integration parameter, as $x = x_p = X_p$ is not any given coordinate. The resulting equations, ordered by their magnitude, take the form:

[3]The same that was said in a previous note for the 2D case, also applies here, and therefore, higher order terms are neglected.

$$O(1): \quad \frac{\mathrm{d}\mathbf{X}_p}{\mathrm{d}t} + \bar{\mathbf{U}} = -\frac{1}{4\pi}\sum_{q=1}^{N}\Gamma_q \int_{-\infty}^{\infty} \frac{(\mathbf{X}_p - \mathbf{X}_q)\times \mathbf{e_x}}{\mid \mathbf{X}_p - \mathbf{X}_q \mid^3}\mathrm{d}x_q \tag{15a}$$

$$\begin{aligned} O(\varepsilon): \quad \frac{\mathrm{d}\mathbf{x'}_p}{\mathrm{d}t} = -\frac{1}{4\pi}\sum_{q=1}^{N}\Gamma_q \int_{-\infty}^{\infty} \Bigg[& \frac{\left((\mathbf{x'}_p - \mathbf{x'}_q)\times \mathbf{e_x} + (\mathbf{X}_p - \mathbf{X}_q)\times \frac{\partial \mathbf{x'}_q}{\partial x_q}\right)}{\mid \mathbf{X}_p - \mathbf{X}_q \mid^3} \\ & - \frac{3 \mid \mathbf{X}_p - \mathbf{X}_q \mid \left((\mathbf{X}_p - \mathbf{X}_q)\cdot(\mathbf{x'}_p - \mathbf{x'}_q)\right)(\mathbf{X}_p - \mathbf{X}_q)\times \mathbf{e_x}}{\mid \mathbf{X}_p - \mathbf{X}_q \mid^6} \Bigg] \mathrm{d}x_q \end{aligned} \tag{15b}$$

$$O(\varepsilon^2): \quad \text{Neglected} \tag{15c}$$

The analysis of the $O(\varepsilon)$ terms will lead to the eigenvalue problem that is used to study the stability of the desired configuration, but before, the satisfaction of the $O(1)$ equation needs to be ensured. As seen in the 2D approach, $\bar{\mathbf{U}}$ might not be zero, but it has to be constant for all vortices. Examples of this kind of motion with constant velocity or angular velocity can be found in Crow [6] and Jiménez [7] respectively. In these examples, the system of reference is moving, and all the points are stationary in that frame. In the case of periodic motion, the stability of the system is studied by means of the Floquet theory as discussed by Crouch [8]. The latter approach consists in the integration of the movement in one period to obtain the matrix of the integrated movement, which is the one used in the eigenvalue problem, but is not considered in the present work. The integration of Eq. (15a) results in exactly Eq. (3a) as the basic state is two dimensional and only the perturbations are allowed to change in the axial direction.

The substitution of $\mathbf{u}(\mathbf{x}_p)$ is not as straightforward as in the 2D case. Here, $\mathbf{u}_p = \mathbf{u}(\mathbf{x}_p) - \bar{\mathbf{U}} = [u_p, v_p, w_p]$, and the derivatives arise from the equation $\mathrm{d}\mathbf{x}_p/\mathrm{d}t + u_p \mathrm{d}\mathbf{x}_p/\mathrm{d}x_p = \mathbf{e_x}u_p + \mathbf{e_y}v_p + \mathbf{e_z}w_p$, where it is observed that x_p is the only directional dependence. It is that because $\mathbf{x}_p(x_p, t) = [x_p, y_p(x_p, t), z_p(x_p, t)]$, as the direction x of the vortex p, x_p, is the only directional dependence, as for every filament p, y_p and z_p are defined. Therefore, $\mathrm{d}\mathbf{x}_p/\mathrm{d}y_p = \mathrm{d}\mathbf{x}_p/\mathrm{d}z_p = \mathrm{d}x_p/\mathrm{d}t = 0$ and the terms $v_p \mathrm{d}\mathbf{x}_p/\mathrm{d}y_p$ and $w_p \mathrm{d}\mathbf{x}_p/\mathrm{d}z_p$ are null. The origin of the previous formula is due to the usage of a fix frame of reference (Eulerian), which is not following the particles, and therefore, the convective term appears. The reader can check that for the 2D case the same formula becomes $\mathrm{d}\mathbf{x}_p/\mathrm{d}t = \mathbf{e_y}v_p + \mathbf{e_z}w_p$, because there is not x dependence as it is for the 3D case. When this equation is linearized, the convective term is of higher order, because $\mathbf{u}_p$ and particularly u_p are of $O(\varepsilon)$ and can be neglected. This is seen when the $O(\varepsilon)$ equations are expanded for each of the three components in scalar form, because there exists a contribution in the x direction, which exposes that $u_p = O(\varepsilon)$:

$$u_p = -\frac{\varepsilon}{4\pi}\sum_{q=1}^{N}\Gamma_q \int_{-\infty}^{\infty} \frac{(Y_p - Y_q)\frac{\partial z'_q}{\partial x_q} - (Z_p - Z_q)\frac{\partial y'_q}{\partial x_q}}{\mid \mathbf{X}_p - \mathbf{X}_q \mid^3}\mathrm{d}x_q \tag{16}$$

The integrals that appear in Eq. (15b) cannot be calculated for a general case because $\mathbf{x'}_q$ are, in general, unknown functions of x_q. However, once exponential perturbations of the form of $\mathbf{x'}_p = \hat{\mathbf{x}}_p \mathrm{e}^{\mathrm{i}kx_p - \mathrm{i}\omega t}$ are assumed, the equations can be integrated, which is done by introducing the new variable $x = x_p - x_q$. These integrals are different for the vortex $p = q$, where a cutoff integral is used, and, therefore, the sum is separated in these cases. d_p is the value of this cutoff for the vortex p, which has to be of the order of the real vortex core size. The integrals are represented using the modified Bessel functions of the second kind $K_0(\alpha)$, $K_1(\alpha)$ and $K_2(\alpha)$ and the cosine integral, $Ci(\alpha)$. Crouch [8] already derived these equations, and Fabre and Jacquin [10] particularized them for aligned vortices. However, the present notation, involves the full equations, highlighting the different variables and parameters on which the equations depend, including the variables $\mathcal{Y}_{pq} = Y_p - Y_q$, $\mathcal{Z}_{pq} = Z_p - Z_q$ and $\zeta_{pq} = \sqrt{(Y_p - Y_q)^2 + (Z_p - Z_q)^2}$, used to simplify the notation. The stability equations in the three-dimensional case read in Cartesian coordinates:

$$-\mathrm{i}\omega\hat{y}_p = \sum_{q=1,p\neq q}^{N} \frac{\Gamma_q}{2\pi}\left[-\frac{\hat{z}_p}{\zeta_{pq}^2} - \frac{k^2K_2(k\zeta_{pq})(\mathcal{Y}_{pq}\hat{y}_q + \mathcal{Z}_{pq}\hat{z}_q)\mathcal{Z}_{pq}}{\zeta_{pq}^2}\right.$$
$$\left. + \left(k^2K_0(k\zeta_{pq}) + \frac{kK_1(k\zeta_{pq})}{\zeta_{pq}}\right)\hat{z}_q + \left(\frac{2(\mathcal{Y}_{pq}\hat{y}_p + \mathcal{Z}_{pq}\hat{z}_p)\mathcal{Z}_{pq}}{\zeta_{pq}^4}\right)\right] \tag{17a}$$
$$+\frac{\Gamma_p}{2\pi}\left[\frac{\cos kd_p - 1 + kd_p\sin kd_p - k^2d_p^2Ci(kd_p)}{2d_p^2}\hat{z}_p\right]$$
$$-\mathrm{i}\omega\hat{z}_p = \sum_{q=1,p\neq q}^{N} \frac{\Gamma_q}{2\pi}\left[\frac{\hat{y}_p}{\zeta_{pq}^2} + \frac{k^2K_2(k\zeta_{pq})(\mathcal{Y}_{pq}\hat{y}_q + \mathcal{Z}_{pq}\hat{z}_q)\mathcal{Y}_{pq}}{\zeta_{pq}^2}\right.$$
$$\left. - \left(k^2K_0(k\zeta_{pq}) + \frac{kK_1(k\zeta_{pq})}{\zeta_{pq}}\right)\hat{y}_q - \left(\frac{2(\mathcal{Y}_{pq}\hat{y}_p + \mathcal{Z}_{pq}\hat{z}_p)\mathcal{Y}_{pq}}{\zeta_{pq}^4}\right)\right] \tag{17b}$$
$$-\frac{\Gamma_p}{2\pi}\left[\frac{\cos kd_p - 1 + kd_p\sin kd_p - k^2d_p^2Ci(kd_p)}{2d_p^2}\hat{y}_p\right]$$

It can be seen that these equations reduce to Eqs. (4) in the two-dimensional limit, $k = 0$. Additionally, the relation between the cutoff d and the size of the vortex a should be stated here, to prevent the reader from misleading the meaning of both of them. Crow [6] showed that the effective core size relation with the cutoff parameter was $d/a_e = 0.6420$ for a Rankine vortex, but other approximations were made by Widnall [57] to match cutoff with any vortex. The relation between the effective radius a_e that appears in the the relation given by Crow and the actual vortex radius a is defined in $\ln(a_e/a) = 1/4 - A + C$, Widnall [57]. In this formula, A and C are represented by the following equations:

$$A = \lim_{\tilde{r}\to\infty}\left[\int_0^{\tilde{r}} r'\tilde{v}_\theta(r')^2dr' - \ln(\tilde{r}/\tilde{a})\right] \qquad C = 2\int_0^{\infty}\tilde{r}\tilde{w}(\tilde{r})^2d\tilde{r} \tag{18}$$

where $\tilde{r}$ in the radial distance, $\tilde{a}$ the vortex radius, $\tilde{v}_\theta(\tilde{r})$ is the swirl velocity and $\tilde{w}(\tilde{r})$ the axial velocity, all non-dimensionalized in the same manner as in it is done for each vortex filament configuration. The Lamb-Oseen vortex, Eq. (19), is chosen later for comparisons with the viscous modal analysis, and then, $A = [\gamma - \ln(2)]/2$ and $C = 0$, where $\gamma \approx 0.5772$, but any other choice is valid. For example, the Rankine vortex, Eq. (20), gives, $A = 1/4$ and $C = 0$.

$$\tilde{v}_{\theta LO}(\tilde{r}) = \frac{1 - \mathrm{e}^{-(\tilde{r}/\tilde{a})^2}}{\tilde{r}} \qquad \tilde{w}_{LO}(\tilde{r}) = 0 \tag{19}$$

$$\tilde{v}_{\theta R}(\tilde{r}) = \tilde{r}/\tilde{a}^2 \quad (\tilde{r} < \tilde{a}) \qquad \tilde{v}_{\theta R}(\tilde{r}) = 1/\tilde{r} \quad (\tilde{r} \geq \tilde{a}) \qquad \tilde{w}_R(\tilde{r}) = 0 \tag{20}$$

The following sections expose a sequence of interesting problems of stability of vortex systems that can be solved by mean of Eqs. (17). Again the configurations of two vortices, counter-rotating as in Crow [6] and co-rotating as in Jiménez [7] and the steady configuration of four vortices studied by Rennich and Lele [9] and Fabre and Jacquin [10] are revisited from a 3D perspective.

2.2.1. Two vortices

1. *Two counter-rotating vortices, Crow [6]*
   The two counter-rotating vortex filaments with homogeneous perturbations along the axial direction are the most interesting configuration, since they provide realistic results (Crow's [6] instability) by means of a very simple model of aircraft wake.
   As it was demonstrated in the analysis of the 2D case, this configuration is in equilibrium in a moving frame of reference, with speed $\bar{\mathbf{U}} = -(\Gamma/2\pi b)\mathbf{e_z}$, and can be used as a steady base flow in the analysis. The parameters are the same as in the 2D analysis ($N = 2$, $p = 1, 2$, $Y_1 = -b/2$, $Y_2 = b/2$, $Z_{1,2} = 0$, $\Gamma_1 = -\Gamma$ and $\Gamma_2 = \Gamma$), and in addition a cutoff parameter $d_1 = d_2 = d$ is considered. All values are substituted into Eqs. (17) and non-dimensionalized, using again the same time ($2\pi b^2/\Gamma$) and distance (b) scales. Two new parameters appear

in the equations, d and $1/k$, which non-dimensionalized give: $\tilde{d} = d/b$ and $\tilde{k} = kb$. The equations are finally written in matrix form using the same nomenclature as before and introducing $\tau(\theta) = \cos\theta - 1 + \theta\sin\theta - \theta^2 Ci(\theta)$ and Bessel functions relations[1]:

$$-\mathrm{i}\tilde{\omega}\begin{pmatrix}\tilde{y}_1\\ \tilde{z}_1\\ \tilde{y}_2\\ \tilde{z}_2\end{pmatrix} = \begin{pmatrix} 0 & 1+\frac{\tau(\tilde{k}\tilde{d})}{2\tilde{d}^2} & 0 & -\tilde{k}^2K_0(\tilde{k}) - \tilde{k}K_1(\tilde{k}) \\ 1-\frac{\tau(\tilde{k}\tilde{d})}{2\tilde{d}^2} & 0 & -\tilde{k}K_1(\tilde{k}) & 0 \\ 0 & \tilde{k}^2K_0(\tilde{k}) + \tilde{k}K_1(\tilde{k}) & 0 & -1-\frac{\tau(\tilde{k}\tilde{d})}{2\tilde{d}^2} \\ \tilde{k}K_1(\tilde{k}) & 0 & -1+\frac{\tau(\tilde{k}\tilde{d})}{2\tilde{d}^2} & 0 \end{pmatrix}\begin{pmatrix}\tilde{y}_1\\ \tilde{z}_1\\ \tilde{y}_2\\ \tilde{z}_2\end{pmatrix} \tag{21}$$

The eigenvalue problem that defines the case of analysis, presented in Eq. (21), was first obtained by Crow [6]. By contrast to the 2D case, the equation depends on two parameters, $\tilde{k}$ and $\tilde{d}$, that have to be defined ahead of the analysis. Once the values of both parameters are set, the solution can be obtained, but caution should be exercised that not every choice of the pair of values will be physically meaningful. Note also that $\tau(\tilde{k}\tilde{d})/\tilde{d}^2$ diverges when $\tilde{d} \to 0$, as the cutoff parameter was needed for the integrals not to diverge. That does not contradict the 2D case, because in that approach, $\tilde{k}$ goes to zero faster than the cutoff distance.
As the cutoff distance d is related to the vortex core size a, following the approach from Crow [6] for the case of the Rankine vortex as an averaged value, $d/a \approx 1/3$. Additionally, the vortex cores are not supposed to interact with each other, and therefore, $b \gg 2a$. These two constraints lead to $\tilde{d} \ll 0.2$.
Furthermore, the length of the oscillation cannot be smaller than the cutoff distance, because it has been removed from the integral. Therefore, an additional restriction should be imposed: $1/\tilde{k} > \tilde{d}$.

2. *Two co-rotating vortices, Jiménez [7]*
The configuration of two co-rotating vortices with homogeneous perturbations in the axial coordinate already analyzed by Jiménez [7] is revisited here. The existence of an equilibrium solution was addressed in the two-dimensional analysis, while stability can be analyzed by solution of Eqs. (17). The pertinent values now are: $N = 2$, $p = 1, 2$, $Z_{1,2} = 0$, $\Gamma_1 = \Gamma_2 = \Gamma$ and $d_1 = d_2 = d$, while $Y_1 = 0$ and $Y_2 = -b$ for vortex 1 and $Y_1 = -b$ and $Y_2 = 0$ for vortex 2. The sign of $\hat{y}_2$ and $\hat{z}_2$ must be changed and a new term has to be introduced, due to the rotation of the system of reference. The same non-dimensionalization scales are used, namely $2\pi b^2/\Gamma$ for time and b for distances. The equations are written as an EVP using the same nomenclature as before:

$$-\mathrm{i}\tilde{\omega}\begin{pmatrix}\tilde{y}_1\\ \tilde{z}_1\\ \tilde{y}_2\\ \tilde{z}_2\end{pmatrix} = \begin{pmatrix} 0 & 1+\frac{\tau(\tilde{k}\tilde{d})}{2\tilde{d}^2} & 0 & -\tilde{k}^2K_0(\tilde{k}) - \tilde{k}K_1(\tilde{k}) \\ -3-\frac{\tau(\tilde{k}\tilde{d})}{2\tilde{d}^2} & 0 & -\tilde{k}K_1(\tilde{k}) & 0 \\ 0 & -\tilde{k}^2K_0(\tilde{k}) - \tilde{k}K_1(\tilde{k}) & 0 & 1+\frac{\tau(\tilde{k}\tilde{d})}{2\tilde{d}^2} \\ -\tilde{k}K_1(\tilde{k}) & 0 & -3-\frac{\tau(\tilde{k}\tilde{d})}{2\tilde{d}^2} & 0 \end{pmatrix}\begin{pmatrix}\tilde{y}_1\\ \tilde{z}_1\\ \tilde{y}_2\\ \tilde{z}_2\end{pmatrix} \tag{22}$$

This equation is the same as the one found by Jiménez [7]. The values of the two parameters $\tilde{k}$ and $\tilde{d}$, need to be chosen in advance of numerical solution of Eq. (22). The same constraints considered in the previous section are also applicable to this section: $\tilde{d}$ should be smaller than around 0.2 (because the vortex cores should be far away) and $1/\tilde{k} > \tilde{d}$ (because the cutoff distance do not consider higher frequency oscillations).

2.2.2. Four aligned vortices, Rennich and Lele [9] and Fabre and Jacquin [10]

The configuration formed by a system of four vortices in equilibrium, as proposed by Rennich and Lele [9], is addressed next. In addition to what was presented in section 2.1.2, homogeneous perturbations in the third direction are permitted. In order to analyze stability, Eqs. (17) are written for $N = 4$, while the remaining parameters have the same values as in the 2D case: $Z_1 = Z_2 = Z_3 = Z_4 = 0$, $Y_1 = -b_1/2$, $Y_2 = -b_2/2 = -\mathcal{X}b_1/2$, $Y_3 = b_2/2 = \mathcal{X}b_1/2$, $Y_4 = b_1/2$, $\Gamma_1 = -\Gamma_0$, $\Gamma_2 = -\mathcal{G}\Gamma_0$, $\Gamma_3 = \mathcal{G}\Gamma_0$, $\Gamma_4 = \Gamma_0$. The relation Eq. (7) between $\mathcal{G}$ and $\mathcal{X}$ is again fulfilled. The same non-dimensionalization as in the 2D case is used: b is the length scale and $2\pi b^2/\Gamma$ the time scale, being

[1] $\mathrm{e}^{(\alpha-1)\pi\mathrm{i}}K_{\alpha-1}(x) - \mathrm{e}^{(\alpha+1)\pi\mathrm{i}}K_{\alpha+1}(x) = \frac{2\alpha}{x}\mathrm{e}^{\alpha\pi\mathrm{i}}K_\alpha(x) \quad \Rightarrow \quad K_0(x) - K_2(x) = -\frac{2}{x}K_1(x)$

$\Gamma = (1+\mathcal{G})\Gamma_0$, $b = (1+\mathcal{X}\mathcal{G})b_1/(1+\mathcal{G})$, $\tilde{\omega} = 2\pi\omega b^2/\Gamma$, $\tilde{x}_i = \hat{y}_i/b$ and $\tilde{y}_i = \hat{z}_i/b$, and, as before, only the range $-1 < \mathcal{G} < 0$ is considered. In addition, new parameters appear because of the three dimensional perturbations: the wavenumber, k, the inner vortex cutoff, d_I, and the outer vortex cutoff, d_O. Their respective non-dimensional values are: $\tilde{k} = bk$, $\tilde{d}_I = d_I/b$ and $\tilde{d}_O = d_O/b$. Finally, the eigenvalue problem $-\mathrm{i}\tilde{\omega}\tilde{\mathbf{x}} = \mathbf{A}\tilde{\mathbf{x}}$ can be written, where $\tilde{\mathbf{x}}$ is the same as in section 2.1.2 and $\mathbf{A}$ will be defined shortly. It depends on $\mathcal{G}$, $\mathcal{X}$, $\tilde{k}$, $\tilde{d}_O$ and $\tilde{d}_I$, which are constant. Here, the same G_i, given in Eqs. (9) are used, as well as $\tau(\theta) = \cos\theta - 1 + \theta\sin\theta - \theta^2 Ci(\theta)$, $K_y(\tilde{k},\theta) = \tilde{k}^2 K_0(\tilde{k}/\theta) + \tilde{k}\theta K_1(\tilde{k}/\theta)$ and $K_z(\tilde{k},\theta) = \tilde{k}\theta K_1(\tilde{k}/\theta)$. For simplicity in the notation and to highlight the different terms, the eigenvalue problem will be written as a function of Ξ_O, Ξ_I, K_{yi} and K_{zi}, defined as:

$$
\begin{aligned}
\Xi_O(\mathcal{G},\tilde{k},\tilde{d}_O) &= \frac{\tau(\tilde{k}\tilde{d}_O)}{2(1+\mathcal{G})\tilde{d}_O^2} \\
\Xi_I(\mathcal{G},\tilde{k},\tilde{d}_I) &= \frac{\mathcal{G}\tau(\tilde{k}\tilde{d}_I)}{2(1+\mathcal{G})\tilde{d}_I^2} \\
K_{yi}(\mathcal{X},\mathcal{G},\tilde{k}) &= \frac{1}{(1+\mathcal{G})} K_y\left(\tilde{k},\ \sqrt{(1+\mathcal{G})G_i}\right) \\
K_{zi}(\mathcal{X},\mathcal{G},\tilde{k}) &= \frac{1}{(1+\mathcal{G})} K_z\left(\tilde{k},\ \sqrt{(1+\mathcal{G})G_i}\right)
\end{aligned}
\tag{23}
$$

With the aid of these quantities, $\mathbf{A}$ becomes:

$$
\mathbf{A} = \begin{pmatrix}
0 & G_5+\Xi_O & 0 & \mathcal{G}K_{y2} & 0 & -\mathcal{G}K_{y1} & 0 & -K_{y3} \\
G_5-\Xi_O & 0 & \mathcal{G}K_{z2} & 0 & -\mathcal{G}K_{z1} & 0 & -K_{z3} & 0 \\
0 & K_{y2} & 0 & G_6+\Xi_I & 0 & -\mathcal{G}K_{y4} & 0 & -K_{y1} \\
K_{z2} & 0 & G_6-\Xi_I & 0 & -\mathcal{G}K_{z4} & 0 & -K_{z1} & 0 \\
0 & K_{y1} & 0 & \mathcal{G}K_{y4} & 0 & -G_6-\Xi_I & 0 & -K_{y2} \\
K_{z1} & 0 & \mathcal{G}K_{z4} & 0 & -G_6+\Xi_I & 0 & -K_{z2} & 0 \\
0 & K_{y3} & 0 & \mathcal{G}K_{y1} & 0 & -\mathcal{G}K_{y2} & 0 & -G_5-\Xi_O \\
K_{z3} & 0 & \mathcal{G}K_{z1} & 0 & -\mathcal{G}K_{z2} & 0 & -G_5+\Xi_O & 0
\end{pmatrix}
\tag{24}
$$

As done by Crouch [8], a new parameter $\tilde{d}$ is defined, which will be equal to the outer vortices non-dimensional cutoff, $\tilde{d} = \tilde{d}_O$. The inner vortices are assumed to follow the relation $\tilde{d}_I = \tilde{d} \mid \mathcal{G} \mid^{1/2}$, which is a consequence of having fixed the vorticity peak and distribution. This choice implies that the only differences in circulation are due to the core size. Of course this is only one possible choice. Others, such as Fabre and Jacquin [10] did not follow this approach, and explicitly took $\tilde{d}_I = 0.5\tilde{d}_O$. However, the assumption of Crouch [8], besides reducing the number of parameters in the problem, is realistic in terms of representation of actual vortex systems and will be used here.

The problem now, has three parameters, $\mathcal{G}$, $\tilde{d}$ and $\tilde{k}$, and will be posed in the following ranges: $-1 < \mathcal{G} < 0$, and $\tilde{d}$ and $\tilde{k}$ given in Figs. 3(a) and 3(b) respectively. The reasons for the choice of range of $\mathcal{G}$ were explained in section 2.1.2. The value of $\tilde{d}$ is a function of the vortex core, and, for the model to be valid, the cores of different vortices should not interact. Two kind of interactions could happen, between outer and inner vortex or between the two inner vortices. For $\mathcal{X} \approx 1$, the first interaction is more probable, while the opposite is the case when $\mathcal{X} \approx 0$. The first case, where the difference between the two centroids should be bigger than the sum of the two vortex cores, that is, for a ratio around one third between cutoff and core size: $(1-\mathcal{X})(1+\mathcal{G})/[2(1+\mathcal{X}\mathcal{G})] > 3\tilde{d}(1+\mid\mathcal{G}\mid^{1/2})$. On the other hand, when the distance between the inner vortices is bigger than the inner vortex diameter, $\mathcal{X}(1+\mathcal{G})/(1+\mathcal{X}\mathcal{G}) > 6\tilde{d} \mid \mathcal{G} \mid^{1/2}$ is considered, again taking the ratio between cutoff and core size to be around one third. The wavenumber $\tilde{k}$ should be given in such a way that the oscillations of the vortex filament have a wavelength bigger than the vortex core, hence, $1/\tilde{k} > \tilde{d}$. In the limits $\mathcal{G} = -1$ and $\mathcal{G} = 0$, $\mathcal{X} = 1$ and $\mathcal{X} = 0$ respectively, and $\tilde{d}$ should be zero as it is shown in Fig. 3(a). That leads to any possible $\tilde{k}$ from Fig. 3(b) and no restriction is applied to the oscillations wavelength.

2.3. Viscous modal linear stability analysis

The inviscid analysis delivers instability results in a rapid and reliable manner if the underlying assumptions are met. However, on occasions these assumptions are found to be restrictive and viscous instability analysis must

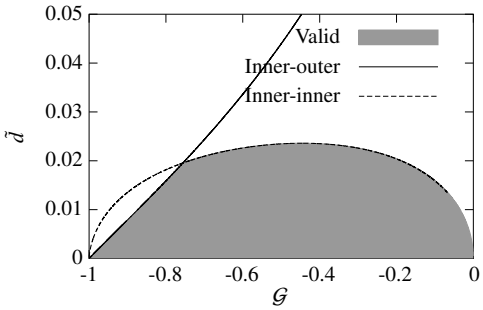

(a) $\tilde{d}$ as a function of $\mathcal{G}$.

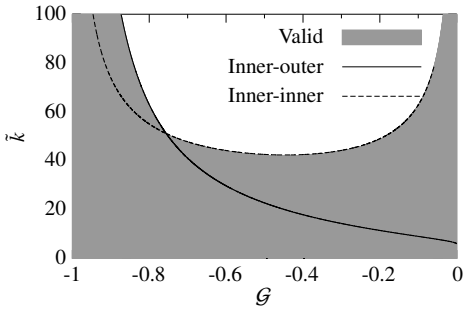

(b) $\tilde{k}$ as a function of $\mathcal{G}$.

Figure 3: Valid values as a function of $\mathcal{G}$, shadow region.

be followed. When the instability analysis of a single vortex is performed, local linear theory could be selected using cylindrical coordinates. Still, since the instability of systems of vortices is addressed, for which there are two inhomogeneous directions, global linear theory must be considered.

By contrast to the inviscid analysis, the starting point of this theory are the Navier-Stokes Equations (NSE), in which the variables, $\bar{\mathbf{q}} = [\bar{\mathbf{u}}, \bar{p}]^T$, are written as the sum of a steady basic state plus a perturbation $\bar{\mathbf{q}}(\mathbf{x}, t) = \mathbf{Q}(\mathbf{x}) + \varepsilon\,\mathbf{q}(\mathbf{x}, t)$ with $\varepsilon \ll 1$. Second order terms are neglected and the Linearized Navier Stokes Equations are obtained:

$$\nabla \cdot \mathbf{u} = 0 \qquad \frac{\partial \mathbf{u}}{\partial t} + \mathbf{U} \cdot \nabla \mathbf{u} + \mathbf{u} \cdot \nabla \mathbf{U} = -\nabla p + \frac{1}{Re}\nabla^2 \mathbf{u} \tag{25}$$

For the problems addressed presently, the axial spatial direction, x, is taken to be homogeneous and the BiGlobal methodology is selected, which uses a 2D basic state $\mathbf{Q} = [U, V, W, P]^T(y, z)$ and assumes a homogeneous dependence upon the third coordinate $\mathbf{q}(x, y, z, t) = [u, v, w, p]^T(x, y, z, t) = \hat{\mathbf{q}}(y, z)\mathrm{e}^{\mathrm{i}(kx-\omega t)}$. The BiGlobal instability analysis equations are written as an eigenvalue problem with $[\hat{u}, \hat{v}, \hat{w}, \hat{p}]^T(y, z)$ as eigenvectors and ω as eigenvalues:

$$\begin{pmatrix} \mathcal{L}_{2D} & U_y & U_z & \mathrm{i}k \\ 0 & \mathcal{L}_{2D} + V_y & V_z & \mathcal{D}_y \\ 0 & W_y & \mathcal{L}_{2D} + W_z & \mathcal{D}_z \\ \mathrm{i}k & \mathcal{D}_y & \mathcal{D}_z & 0 \end{pmatrix} \begin{pmatrix} \hat{u} \\ \hat{v} \\ \hat{w} \\ \hat{p} \end{pmatrix} = \begin{pmatrix} \mathrm{i}\omega & 0 & 0 & 0 \\ 0 & \mathrm{i}\omega & 0 & 0 \\ 0 & 0 & \mathrm{i}\omega & 0 \\ 0 & 0 & 0 & 0 \end{pmatrix} \begin{pmatrix} \hat{u} \\ \hat{v} \\ \hat{w} \\ \hat{p} \end{pmatrix}, \tag{26}$$

where $\mathcal{L}_{2D} = U\mathrm{i}k + V\mathcal{D}_y + W\mathcal{D}_z - \frac{1}{Re}(-k^2 + \mathcal{D}_{yy} + \mathcal{D}_{zz})$.

The interested reader is referred to Hein and Theofilis [35], Jacquin et al. [36] and Theofilis [32] for details. The numerical solution of Eq. (26) is discussed by Paredes et al. [66]. Symmetry boundary conditions are imposed at the mid-plane, such that half of the domain needs to be computed and different Lamb-Oseen vortices are used to construct the basic flow in different situations. For details of the basic flow equations, the boundary conditions and other mesh properties, the reader is referred to Tendero et al. [67, 68].

In order for viscous and inviscid vortex-filament analysis results to be compared, the cutoff, d used in the filament methods and the size of the vortex a, used as a basic flow for the viscous modal analysis, need to be related. Details of the relationships are given at the end of section 2.2 and Eq. (18) taken from Widnall [57]. Unless other thing is stated, the Lamb-Oseen vortex model is chosen for the viscous modal analysis, although others as the Rankine vortex, the q-vortex, or any other choice is reasonable. The usual definition of Reynolds number, $Re = \Gamma/2\pi\nu$, with ν the kinematic viscosity, is used in the viscous analysis.

3. Results

In this section results of the inviscid eigenvalue problems presented are shown for a number of well-known vortex system configurations and comparisons with viscous linear stability theory are shown, highlighting the limit of appli-

cability of the inviscid theory. The significance of the works presented by von Kármán [3, 4], Crow [6], Jiménez [7], Crouch [8], Rennich and Lele [9] and Fabre and Jacquin [10] has been already highlighted and the respective configurations are selected for the presentation. When comparing viscous and inviscid analysis results, an attempt is made to explain both of the situations in which agreement and disagreement between the two theories can be found.

3.1. Two dimensional stability analysis

3.1.1. Two vortices

1. *Two counter-rotating vortices, Crow [6]*
   Solving Eq. (5) analytically, only one quadruple eigenvalue $-\mathrm{i}\tilde{\omega} = 0$ is obtained. The physical explanation of this trivial results is that if any perturbation is introduced on the initial positions, it will be neutrally stable and the system will equilibrate in the new position.
2. *Two co-rotating vortices, Jiménez [7]*
   Solution of Eq. (6) now results in one double eigenvalue $-\mathrm{i}\tilde{\omega} = 0$ and two complex conjugates $-\mathrm{i}\tilde{\omega} = \pm 2\mathrm{i}$. In mathematical terms the zero real part of the eigenvalue again implies neutral stability, which manifests itself in physical terms as a situation in which two co-rotating vortices moved from their original positions, continue forming a displaced system of two vortices rotating around the centroid.

3.1.2. Four aligned vortices, Rennich and Lele [9] and Fabre and Jacquin [10]

The eigenvalues $\tilde{\omega}$ in Eq. (8) are calculated as a function of the circulation ratio $\mathcal{G}$. Fig. 4 shows the variation, where $\tilde{\omega}_i \to \infty$ as $\mathcal{G} \to -1$, which means that in that limit this configuration is very unstable: the vortices are very near to each other and any small perturbation of the position will change their relative positions by a very large amount. This limit is actually also prone to larger errors in the computation of the eigenvalues.

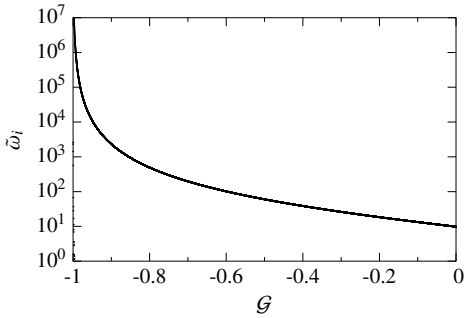

Figure 4: Amplification rate $\tilde{\omega}_i$ as function of the circulation ratio $\mathcal{G}$ for the four vortices in equilibrium configuration.

The configuration becomes less unstable when $\mathcal{G} \to 0$. This limit ($\mathcal{G} = \mathcal{X} = 0$) is actually the same as that of a two-vortex configuration. However, although the eigenvalues corresponding to a two-vortex system in which $\mathcal{G} = 0$ are $\tilde{\omega} = 0$, this is not the case when the two-vortex system is approached as a limit-case of the four-vortex configuration. The explanation of this contradiction, is that the modes associated with the non-zero eigenvalues only affect the inner and weaker vortices. In the limit, they are infinitely weak and do not really exist, and therefore, the mode itself does not really exist for $\mathcal{G} \to 0$. The value of the amplification rate in the case $\mathcal{G} = \mathcal{X} = 0$ is increasingly challenging to obtain numerically because the problem becomes singular. It can be solved analytically by means of Taylor series, and two double eigenvalues $\tilde{\omega}_i = \pm 4\sqrt{6}$ (9.79795897...) appear, in addition to the quadruple zero eigenvalue. As $\tilde{\omega}_r = 0$, all modes are stationary, so only the amplification rate ($\tilde{\omega}_i$) is shown in Fig. 4.

3.1.3. Infinite row of vortices, von Kármán [3, 4]

1. *Equidistant aligned vortices rotating in the same sense*
   In this case, the eigenvalues are $-\mathrm{i}\tilde{\omega} = \pm f_1(\varphi)$. Therefore, there exist one positive and one negative real values and the configuration is unstable due to the positive one. The eigenvector associated with the positive eigenvalue is $(\tilde{y}_0, \tilde{z}_0) = (1, -1)$, which means that the vortices will move in directions forming an angle of 45

degrees with the original vortex line. Furthermore, the maximum value of $f_1(\varphi = \pi) = \pi^2/4$, resulting in $\tilde{\omega}_{i,max} = \pi^2/4 \approx 2.4674$, which means that the higher growth appears for periods of two vortices. The most unstable mode is a pair of vortices moving in the directions $(\tilde{y}_0, \tilde{z}_0) = (1, -1)$ and $(\tilde{y}_0, \tilde{z}_0) = (-1, 1)$ alternatively, which is actually the Kelvin-Helmholtz instability.

2. *Equidistant aligned vortices rotating in alternating senses*
The eigenvalues of the problem are $-\mathrm{i}\tilde{\omega} = \pm \mid f_2(\varphi) \mid$, and this configuration is also unstable due to the positive value. $f_2(\varphi) \leq 0$ with a very sharp maximum absolute value at $\varphi = \pi$. The positive growing eigenvalue is $\tilde{\omega}_i = -f_2(\varphi)$ and the corresponding eigenvector $(\tilde{y}_0, \tilde{z}_0) = (1, 1)$. $f_2(\pi) = -\pi^2/4$ and therefore, $\tilde{\omega}_{i,max} = \pi^2/4 \approx 2.4674$, the same as in the previous case.
3. *Two rows of equidistant aligned vortices rotating in the same sense, one on top of the other* (Stability not addressed)
4. *Two rows of equidistant aligned vortices rotating in opposite senses, one on top of the other, von Kármán [4]*
The eigenvalues for this case have the form $-\mathrm{i}\tilde{\omega} = \pm(B_1 \pm \sqrt{A_1^2 - C_1^2})$. B_1 has only imaginary part, so the real part, if present, would come from the therm inside the square root. Therefore, if $\mid A_1 \mid > \mid C_1 \mid$, there will be two eigenvalues with negative real part and two with positive real part ($\tilde{\omega}_i = \pm\sqrt{A_1^2 - C_1^2}$, $\tilde{\omega}_r = \pm B_1/\mathrm{i}$), and the configuration will be unstable due to them. On the other hand, if $\mid A_1 \mid \leq \mid C_1 \mid$ the four eigenvalues will only have imaginary part ($\tilde{\omega}_i = 0$, $\tilde{\omega}_r = \pm(B_1/\mathrm{i} \pm \sqrt{C_1^2 - A_1^2})$) and the configuration will be neutrally stable. However, A_1 is maximum for $\varphi = \pi$, and for that value, $A_1^2 - C_1^2 = \pi^4/16 > 0$ independent of l/e. That means that the configurations is always unstable to perturbations to vortex pairs for every choice of l/e. The value of the growth rate for the most amplified mode is then $\tilde{\omega}_{i,max} = \pi^2/4$, and, additionally, $B_1 = 0$ for $\varphi = \pi$ and the mode is double and non-travelling ($\tilde{\omega}_r = 0$).
5. *Two rows of equidistant aligned vortices rotating in the same sense, displaced half distance* (Stability not addressed)
6. *Two rows of equidistant aligned vortices rotating in opposite senses, displaced half distance, von Kármán [4]*
This time the eigenvalues are $-\mathrm{i}\tilde{\omega} = \pm(B_2 \pm \sqrt{A_2^2 - C_2^2})$ and therefore, if $\mid A_2 \mid > \mid C_2 \mid$, the configuration will be unstable and if $\mid A_2 \mid \leq \mid C_2 \mid$ the configuration will be neutrally stable. Selecting once more $\varphi = \pi$, ($N = 2$), it is found that $C_2 = 0$, and $\mid A_2 \mid > \mid C_2 \mid$, unless $A_2 = 0$, which occurs for $l/e \approx 3.564$, solution of $\cosh(\pi e/l) = \sqrt{2}$. This selection gives neutral stability, and every other choice of the parameter l/e produces growth, whose rate is function of the same parameter, $\tilde{\omega}_{i,max} = \pi^2/4 \mid 1 - 2\cosh^2(\pi e/l) \mid$. The modes will have frequency as a general basis ($\tilde{\omega}_r \neq 0$).

3.2. Three dimensional stability analysis

3.2.1. Two vortices

1. *Two counter-rotating vortices, Crow [6]*
The stability of the counter-rotating vortices is governed by Eq. (21). The eigenvalue problem is solved for six selections of $\tilde{d}$: 10^{-6}, 0.001, 0.1, 0.2, 0.3 and 0.4, which cover most of the range in which the methodology is applicable. The results are shown for the first three values in the range $0 < \tilde{k} < 2$, as the eigenvalues are zero for higher values inside the region of validity of the method, see Figs. 5(a), 5(b) and 5(c). For the last three choices of $\tilde{d}$, the range $0 < \tilde{k} < 6$ is examined, although some of the values shown are in the area out of bounds, which is shown shadowed in the figures. In fact, these three values of cutoff, Figs. 5(d), 5(e) and 5(f), are outside of the region of validity for $\tilde{d}$, but they have been reproduced because they are similar to figure 9 of Crow [6], and include the shadowing of the non eligible area. There are two symmetric modes that come closer as $\tilde{d}$ increases, becoming a single mode at $\tilde{d} \approx 0.25$. An antisymmetric mode also exists, which approaches $\tilde{k} = 0$ for larger values of $\tilde{d}$. Although this is the leading mode, its maximum is always outside of the range of validity of the method. For the area of realizable results, a single symmetric mode, known as Crow mode, grows from $\tilde{k} = 0$, having a maximum for a value of $\tilde{k}$ dependent of $\tilde{d}$, but always in the segment of $0 < \tilde{k} < 1$ (in the range of values considered). The maximum amplification rate of the mode is always in the range 0.5 to 1, varying little with changes of the cutoff parameter.

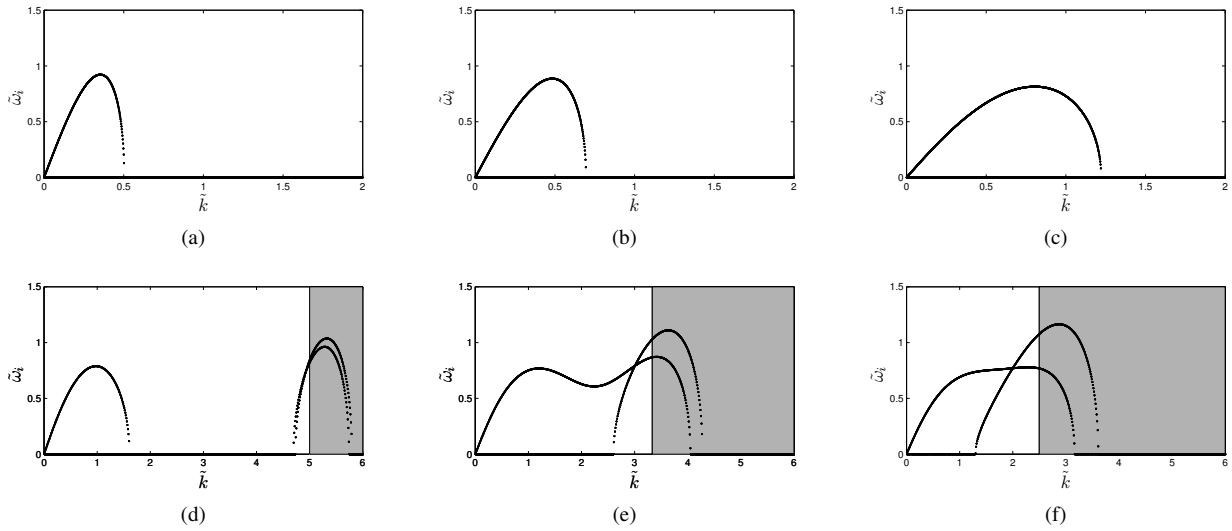

Figure 5: Amplification rate $\tilde{\omega}_i$ as a function of the wavenumber $\tilde{k}$ for $\tilde{d}$: (a) 10^{-6}, (b) 0.001, (c) 0.1, (d) 0.2, (e) 0.3 and (f) 0.4. (d) to (f) same as Crow [6] Fig. 9, highlighting the area out of bounds for high wavenumbers.

The four eigenvalues are always in pairs and are either real or imaginary. The couples have the same value with positive and negative sign. That is, when there is a growing mode, there exists a decaying mode, and the neutral eigenvalues appear always in pairs of positive and negative frequency.
The shape of the modes is introduced with the help of Figs. 6 and 7. Fig. 6 has been chosen within the range of validity of the method, $\tilde{k} = 0.5$ and $\tilde{d} = 0.001$, where the only growing mode is the symmetric Crow mode, Fig. 6(a). On the other hand, Fig. 7 represents a case with two growing modes, symmetric Crow mode Fig. 7(a) and antisymmetric non realizable Fig. 7(c), outside of the valid region for the cutoff parameter, $\tilde{k} = 2$ and $\tilde{d} = 0.4$. Note here that the limits that have been taken both for $\tilde{k}$ and $\tilde{d}$ are diffuse, and the antisymmetric growing mode might be realistic in some cases. Its growth rate is also high, so it might compete with the symmetric growing mode if some particular wavelengths are excited. The symmetric growing mode is present in both Figs. 6(a) and 7(a). In the regions that either the symmetric or antisymmetric mode are neutrally stable, two modes with frequency appear, that neither grow nor decay, but move at a finite frequency in time both upstream and downstream. The antisymmetric modes represented in Figs. 6(c) and 6(d) are examples of neutral modes.

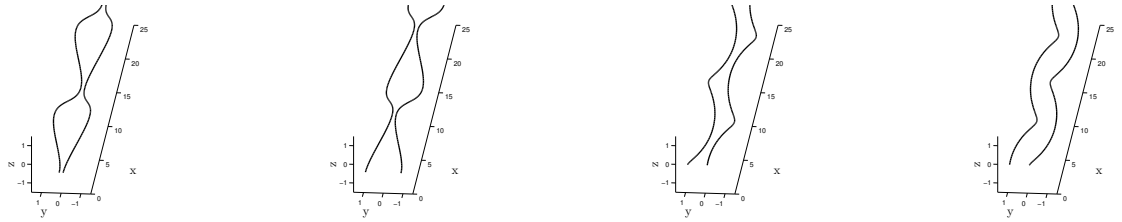

(a) Symmetric, growing (Crow). (b) Symmetric, decaying. (c) Antisymmetric, positive. (d) Antisymmetric, negative.

Figure 6: The four modes for $\tilde{k} = 0.5$ and $\tilde{d} = 0.001$. One growing (Crow mode), one decaying and two neutral.

It is also worth mentioning that the amplification rate and frequency are zero for the limit of wavenumber approaching to zero, as seen in Fig. 5, which is in agreement with the two-dimensional analysis.

2. *Two co-rotating vortices, Jiménez [7]*
The instability analysis of the co-rotating vortices is performed through the study of the eigenvalues of Eq. (22). This configuration is stable for the range of parameters considered, $\tilde{d} \leq 0.2$ and $1/\tilde{k} > \tilde{d}$. There are two unstable

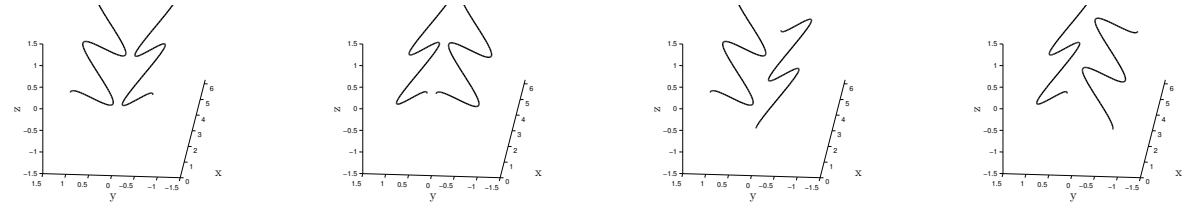

(a) Symmetric, growing (Crow). (b) Symmetric, decaying. (c) Antisymmetric, growing. (d) Antisymmetric, decaying.

Figure 7: The four modes for $\tilde{k} = 2$ and $\tilde{d} = 0.4$. Two growing and two decaying.

modes, with their respective stable modes, symmetric and antisymmetric for a range of wavenumbers $\tilde{k}$ slightly higher than the range $1/\tilde{k} > \tilde{d}$, but because they are out of the range of validity of the method, their existence cannot be justified. These two modes appear almost for the same range of wavenumbers: the symmetric is the first to appear and the more unstable of the two, having a maximum value of $\tilde{\omega}_i$ slightly larger than unity and varying slightly for cutoff parameter $\tilde{d}$ variations.
In the rest of the wavenumber range (the valid one), there are always four neutral modes in pairs, symmetric and antisymmetric. The higher frequency is always for the antisymmetric, whose value is two in non-dimensional values for $\tilde{k} = 0$ and any $\tilde{d}$, which corresponds to the 2D case. The value of the frequency of this mode grows as the wavenumber increases, reaching a maximum just before the end of validity of the approach and depending on the cutoff parameter. The symmetric mode has a similar behavior, having a smaller frequency than the antisymmetric mode. In the limit of $\tilde{k} \to 0$, $\tilde{\omega}_i \to 0$ and $\tilde{\omega}_r \to 0$ or ± 2, which coincides with the 2D case.

3.2.2. Four aligned vortices, Rennich and Lele [9] and Fabre and Jacquin [10]

The results of the Rennich and Lele [9] configuration of section 2.2.2 are analyzed here from a three-dimensional point of view. In addition, as a cross-validation of the results presented earlier for two vortices, calculations are performed for $\mathcal{G} = -10^{-5}$ and the results are compared with those of the two counter-rotating vortices configuration. If the figures of the two vortices (Figs. 5) are compared with figures for the four vortex approach, four modes are indistinguishable, and other four modes appear, some of them much more unstable, but affecting the inner vortices, which are very weak in that limit. As an example, the values of $\tilde{\omega}_i$ for $\tilde{k} = 3.5$ are compared in both cases for the two Crow eigenvalues in table 1, in which $\tilde{d} = 0.3$ is chosen. This value is well outside the validity region of the method, but the objective here is to cross-verify that the two configurations deliver analogous results.

Mode	$\tilde{\omega}_i$ 2 Vortices	$\tilde{\omega}_i$ 4 Vortices	Relative Error
Antisymmetric	1.092960238456726	1.092994599627738	3.14×10^{-05}
Symmetric	0.8669134974479675	0.8669361404957115	2.61×10^{-05}

Table 1: Comparison of amplification rates $\tilde{\omega}_i$ for 2 and 4 vortices taking $\mathcal{G} = -10^{-5}$ in the 4 vortex problem, $\tilde{k} = 3.5$ and $\tilde{d} = 0.3$.

Results of the 3D approach should also converge to those of the 2D approach when the wavenumber is taken very small. This has been checked for $\tilde{k} = 10^{-3}$, where the values for 2D ($\tilde{k} = 0$) are recovered. Table 2 compares the value of the non-zero eigenvalue both for the 2D problem and in the limit of the 3D when both $\mathcal{G}$ and $\tilde{k}$ are close to zero for $\tilde{d} = 0.3$, as other values of the cutoff will show similar agreement. Here, the 4 values (two positive and two negative) obtained numerically are not equal, therefore, only the digits that are common are presented.

$\tilde{\omega}_i$ 2D Analytic	$\tilde{\omega}_i$ 3D $\tilde{k} = 10^{-3}$	Relative Error
9.797958971132712	9.7982...	2.46×10^{-05}

Table 2: Comparison of amplification rates $\tilde{\omega}_i$ for 4 vortices, both 2D and 3D when both problems approach as $\tilde{k}$ tends to zero. $\mathcal{G} = 0$ in the 2D problem and $\mathcal{G} = -10^{-5}$ and $\tilde{d} = 0.3$ in the 3D problem.

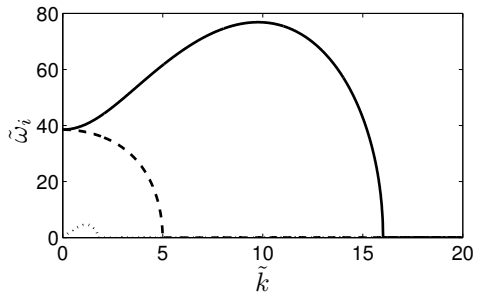

Figure 8: Amplification rate $\tilde{\omega}_i$ as a function of the wavenumber $\tilde{k}$ for $\tilde{d} = 0.02$ and $\mathcal{G} = -0.4$. Solid line: symmetric mode for inner vortices Fig. 9(a). Dashed line: antisymmetric mode for inner vortices Fig. 9(b). Dotted line: the Crow mode for the entire vortex system Fig. 9(c).

Attention is now turned to the 4-vortex system, in which finite values of $\mathcal{G}$ are considered. The pair of parameters $\tilde{d} = 0.02$ and $\mathcal{G} = -0.4$ is considered, which is in the upper limit for the vortex core taken from Fig. 3(a), where, as seen in Fig. 3(b), $\tilde{k}$ can take values from 0 to approximately 40. Fig. 8 shows the amplification rate, where only the range of wavenumbers from 0 to 20 is shown, as all the eigenvalues are neutral above this limit. In that range, there exist three unstable modes. The highest of them is symmetric, solid line in Fig. 8, shown in Fig. 9(a), where it can be seen that is a mode affecting mainly the inner vortices. The second in amplification (dashed line in Fig. 8, Fig. 9(b)) is antisymmetric, has similar growth rate as the symmetric mode and also affects more the inner vortices. In the limit $\tilde{k} \to 0$ these two modes merge together. The values of the amplification rates of these modes are rather high, which highlights how unstable the configuration is. The third mode in amplification, is the Crow mode for the entire vortex system, dotted line in Fig. 8. Its amplification is one order of magnitude lower, and its region of instability is much smaller than the modes discussed previously, but it is significant in terms of aircraft wake destruction, as it also affect the outer vortices. These three modes have their respective decaying counterparts, while two neutral modes also exist in that region, all shown in Fig. 9.

Finally, results corresponding to $\tilde{d} = 0.01$ are discussed. In this case, Fig. 3(b) shows that nearly the entire range of $\mathcal{G}$ is available. The amplification rate is calculated as function of the wavenumber for various values of the circulation ratio. The qualitative shape of the results is similar to Fig. 8, so they are not plotted again. However, they have important quantitative differences with the results shown in Fig. 8. The amplification of the three unstable modes grows to very large values as $\mathcal{G} \to -1$. The non-dimensional maximum value of amplification rate of the most unstable mode is around 100 for small values of $\mathcal{G}$, reaching 150 for intermediate values of the circulation ratio and growing very rapidly as $\mathcal{G} \to -1$. The region of unstable wavenumbers also increases in general with higher values of the absolute value of $\mathcal{G}$. Only one qualitative change occurs for $\mathcal{G} = -0.7$ and below, which is that the second mode has also a maximum.

Fabre and Jacquin [10] performed analogous analysis of the four-vortex system, but they related directly the results with the vortex radius, and did not use the cutoff assumption. Their approach, although is more realistic, particularly for high wavenumbers where the cutoff assumption is not valid, makes the methodology dependent of the choice of vortex model (in their case the Rankine vortex model) and it has been the reason not to use it here, where the approach taken is independent of the vortex model. It is worth to highlight here that the choice of cutoff done in the present work, allows to compare the filament results with results using any vortex model, using the formulas of Widnall [57] to convert cutoff distance into vortex radius, known the vortex shape. They used the following values, in the notation of this work, $\tilde{d}_O = 0.0409$, $\tilde{d}_I = 0.0204$ and $\mathcal{G} = -0.4$, and they did not use the Crouch [8] assumption ($\tilde{d}_I = \tilde{d}_O \mid \mathcal{G} \mid^{1/2}$). In order to compare the results of Fabre and Jacquin [10] with those of the present methodology, here kb_1 needs to be multiplied by 1.57 to obtain $\tilde{k}$ and $(2\pi b_1/\Gamma)\sigma_r$ by 4.11 to obtain $\tilde{\omega}_i$. Doing so, the results of the two approaches are indistinguishable up to high values of wavenumber, where their solution is predicted to be more unstable than that presented herein.

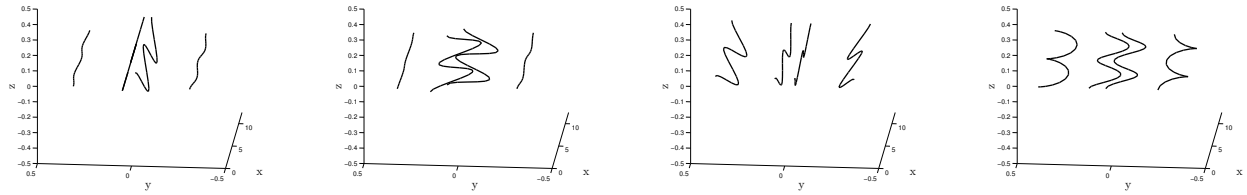

(a) Symmetric 1, growing. (b) Antisymmetric, growing. (c) Symmetric 2, growing. (d) Antisymmetric, neutral P.

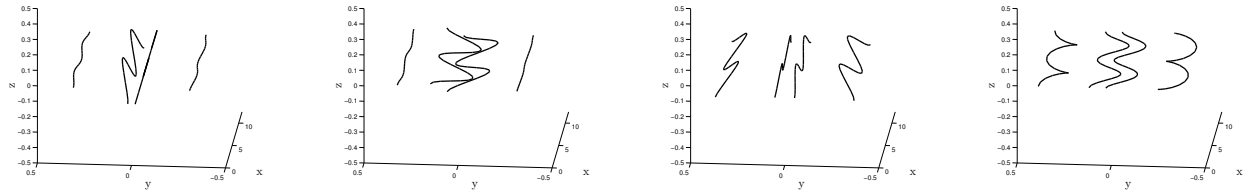

(e) Symmetric 1, decaying. (f) Antisymmetric, decaying. (g) Symmetric 2, decaying. (h) Antisymmetric, neutral N.

Figure 9: The eight modes for $\tilde{k} = 1$, $\tilde{d} = 0.02$ and $\mathcal{G} = -0.4$. Three growing, three decaying and two neutral eigenvalues.

3.3. Comparison between inviscid vortex filaments and viscous linear stability theory

Finally, viscous linear stability theory is considered and results of its predictions are compared with those delivered by the inviscid analysis. There are several works that have applied viscous modal analysis to vortical flows among which only a few addressed the issue of direct comparisons between inviscid, vortex-filament-based, and viscous linear stability analysis; the present work intends to provide such a comparison.

3.3.1. Two counter-rotating vortices

Two sets of parameters have been examined, ($\tilde{d} = 0.1$, $\tilde{a} = 0.1145$) and ($\tilde{d} = 0.2$, $\tilde{a} = 0.2290$), where $\tilde{a} = a/b$ is the non-dimensional vortex core radius, not defined earlier, but using again b for the non-dimensionalization purpose in this case and $\sim$ for non-dimensional values. The correspondence between $\tilde{d}$ and $\tilde{a}$ given by the Widnall [57] formulas: $\tilde{a} = \tilde{d}/(0.6420\mathrm{e}^{1/4-A+C})$ and Eq. (18), particularized A and C for the Lamb-Oseen vortex model. In the results shown in what follows, $Re = 1000$ was found to be a good compromise between obtaining Reynolds-independent amplification rates while maintaining the cost of solution of Eq. (26) tractable. Results are shown in Fig. 10, where it can be observed that the matching between the results delivered by the two approaches is much better for the first choice of parameters. The explanation for this behavior is that the second set of parameters corresponds to vortices that are closer together than those corresponding to the first choice of parameters. At the relatively low Reynolds number value chosen, viscous diffusion makes the idealized inviscid model questionable in that case. Benton and Bons [69] found a similar behavior in their analysis, the comparison between the two approaches being relatively good when the vortices are far apart, but viscous analysis results depart from those of the inviscid vortex filament theory as the vortices come closer. By contrast, Brion et al. [70] obtained excellent agreement between results delivered by the two approaches even when the two vortices are rather close. However, they used a DNS calculated basic flow, and most probably a better adjustment for the vortex radius, both for the viscous and the inviscid calculations. Despite of that, the results still prove both methodologies to produce reliable results when the vortices are not very close. The limit of validity of these good matching is between $\tilde{d} = 0.1$ ($\tilde{a} = 0.1145$) and $\tilde{d} = 0.2$ ($\tilde{a} = 0.2290$).

Fig. 11 presents a superposition of the instability analysis results delivered by the two methodologies at a value of the wavenumber parameter $\tilde{k} = 0.8$, which corresponds to the maximally amplified perturbation in both analyses. The superposition of the base flow vorticity and that of the leading eigenmode at a linearly small amplitude parameter, $\varepsilon = 0.1$ is plotted. Lines represent the vortex filament result, while the viscous eigenmode is shown with a finite vortex

radius. The direction x of the homogeneous perturbation is scaled to show the vortices in a more compact way, as the wavenumber is very small. From a numerical point of view, introduction of viscosity raises the 3 sec computing time needed for the recovery of the inviscid result to nearly 6 minutes per wavenumber analysis, while the memory needed for the viscous instability work is orders of magnitude larger than that used in the inviscid analysis.

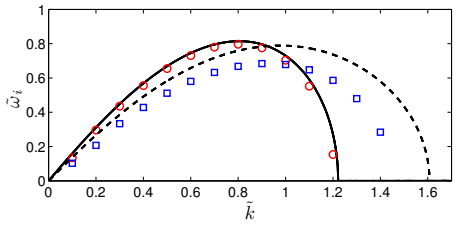

Figure 10: Comparison between filament (lines) and BiGlobal theory at $Re = 1000$ (points). Amplification rate $\tilde{\omega}_i$ as a function of the wavenumber $\tilde{k}$ for $\tilde{d} = 0.1$ and $\tilde{a} = 0.1145$ (solid line and circles) and $\tilde{d} = 0.2$ and $\tilde{a} = 0.2290$ (dashed line and squares).

Figure 11: Basic flow plus perturbation for the leading mode at $\tilde{k} = 0.8$ comparison between the filament positions obtained from the vortex filament stability analysis at $\tilde{d} = 0.1$ (lines) and the vorticity isosurfaces obtained from the BiGlobal analysis for $Re = 1000$ and $\tilde{a} = 0.1145$ (surfaces). Perpendicular direction not scaled.

In order to check the dependence with the vortex model, two cases have been selected, where the viscous BiGlobal is performed both for the Lamb-Oseen (LO) and the Rankine (R) vortex, as well as the inviscid filaments methodology is also compared. Table 3 shows this comparison for two vortex sizes, $\tilde{d} = 0.1$ ($\tilde{a} = 0.1145$ for LO and $\tilde{a} = 0.1558$ for R) and $\tilde{k} = 0.8$, as well as $\tilde{d} = 0.2$ ($\tilde{a} = 0.2290$ for LO and $\tilde{a} = 0.3115$ for R) and $\tilde{k} = 1.0$, both near to the maximum growth rate of the mode for each vortex size. The Reynolds number is kept the same for the viscous simulations ($Re = 1000$). Both viscous vortex models show degradation of agreement for the vortices with greater cores with respect to the inviscid case. For the two selections of vortex size, the agreement between Rankine and inviscid is better than between Lamb-Oseen and inviscid, but always of the same order.

$\tilde{d}$	$\tilde{k}$	$\tilde{\omega}_i$ Inviscid	$\tilde{\omega}_i$ Viscous LO	$\tilde{\omega}_i$ Viscous R	Relative Difference with Inviscid, LO/R
0.1	0.8	0.8145...	0.7969...	0.8049...	$2.17 \times 10^{-02}/1.18 \times 10^{-02}$
0.2	1.0	0.7883...	0.6782...	0.7036...	$1.40 \times 10^{-01}/1.07 \times 10^{-01}$

Table 3: Comparison of amplification rates $\tilde{\omega}_i$ for inviscid and viscous ($Re = 1000$) methodologies, showing the vortex model dependence for the two counter-rotating vortex system selecting two different vortex sizes: $\tilde{d} = 0.1$ ($\tilde{a} = 0.1145$ for LO and $\tilde{a} = 0.1558$ for R), $\tilde{k} = 0.8$ and $\tilde{d} = 0.2$ ($\tilde{a} = 0.2290$ for LO and $\tilde{a} = 0.3115$ for R), $\tilde{k} = 1.0$, always for the Crow mode (symmetric).

3.3.2. Four aligned vortices

The case is solved for the set of parameters previously addressed, $\tilde{d} = 0.02$, $\mathcal{G} = -0.4$. The corresponding value for the vortex radius is then $\tilde{a} = 0.0229$ in the viscous analysis. At $Re = 1000$ only the Crow mode of the outer vortices corresponds to the result of the to the inviscid theory. At $Re = 10000$ the remaining modes known from the inviscid analysis also appear in the viscous eigenspectrum. At high Reynolds number values the viscous instability analysis delivers an increasingly large number of spurious eigenmodes and also the characteristics of the leading perturbations are qualitatively different between the two types of analysis: from the three modes recovered, the leading mode (symmetric and only affecting the inner vortices) is found to have a nonzero frequency in the viscous analysis, while the inviscid theory predicts this mode to be stationary. A number of parameters, whose selection is guided by the results of Fig. 8, have been chosen in order to perform the viscous global linear instability work. The choices made are shown as discrete points in Fig. 12, alongside the full lines of inviscid results, reproduced from Fig. 8. In all cases shown, very good agreement between the results of the two types of analysis is obtained. Although the value $\tilde{d} = 0.02$ might seem small, from Fig. 3(a) is can be seen that is actually in the limit of validity of the approach. To show this fact, a value slightly higher of vortex core, $\tilde{a} = 0.025$, equivalent to $\tilde{d} = 0.0218$ is calculated. Table 4 compares results obtained from the filament inviscid instability and BiGlobal viscous instability for the particular case $\tilde{k} = 1.8$ and antisymmetric mode, given $\tilde{d} = 0.02$ ($\tilde{a} = 0.0229$) and $\tilde{d} = 0.0218$ ($\tilde{a} = 0.025$) both for $\mathcal{G} = -0.4$. It is observed how

a very little change of vortex size leads to an increase of the disagreement between the two approaches from less than 1% for $\tilde{a} = 0.0229$ to almost 10% for $\tilde{a} = 0.025$.

$\tilde{a}$	$\tilde{\omega}_i$ Inviscid	$\tilde{\omega}_i$ Viscous	Relative Difference
0.0229	36.189...	36.423...	6.45×10^{-03}
0.025	36.623...	33.047...	9.76×10^{-02}

Table 4: Comparison of amplification rates $\tilde{\omega}_i$ for inviscid and viscous ($Re = 10000$) methodologies for the four vortex system selecting $\mathcal{G} = -0.4$ and $\tilde{k} = 1.8$ and two choices of $\tilde{d} = 0.02, 0.0218$ ($\tilde{a} = 0.0229, 0.025$), for the antisymmetric mode.

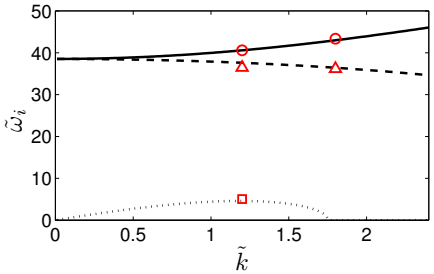

Figure 12: Comparison between inviscid (lines) and viscous linear theory results for the amplification rate $\tilde{\omega}_i$ as a function of wavenumber $\tilde{k}$ for $Re = 10000$ (points). $\tilde{d} = 0.02$ and $\tilde{a} = 0.0229$. Solid line and circles: symmetric mode inner vortices. Dashed line and triangles: antisymmetric mode inner vortices. Dotted line and circle: symmetric Crow mode.

Figure 13: Basic flow plus $\varepsilon = 0.02$ perturbation for the second symmetric mode at $\tilde{k} = 1.2$ comparison between the filament positions obtained from the inviscid analysis at $\tilde{d} = 0.02$ (lines) and the vorticity isosurfaces obtained from the BiGlobal analysis for $Re = 10000$ and $\tilde{a} = 0.0229$ (surfaces). Perpendicular direction not scaled.

4. Summary

The inviscid instability analysis methodology based on point vortices (2D) and vortex filaments (3D) is presented in a unified manner. Instability is solved for systems of two vortices [6, 7], for the Rennich and Lele [9] four-vortex system, as well as for sets of infinite aligned vortices as those analyzed by von Kármán [3, 4].

Effort is paid to identify and expose the assumptions underlying this theoretical approach in terms of the permissible parameters in the analysis. Subsequently, the more complete (and computationally orders-of-magnitude more expensive) viscous linear instability theory is also employed to analyze some of the most interesting configurations. Results of the two approaches are generally found to be in agreement with each other, as long as the vortices are not very close, so the filament approach is valid, even when Reynolds number is maintained in moderate values for the viscous analysis. Therefore, the main limitation of the inviscid approach is the impossibility of analyzing vortices whose size is comparable to their distance, as well as very large wavenumbers, which imply very short wavelengths, although the last of them can be overcome by different strategies. In addition, viscosity cannot be introduced, but on the contrary, this methods can analyze inviscid configurations, while the viscous methods tent to fail more when the viscosity is low. The viscous methods can analyze closer vortices and larger wavenumbers, but on the other side, they are orders of magnitude more demanding of computational resources, which is the main advantage of the inviscid methods, which some times can be solved even analytically.

The present work includes several novel features, embedded among other previous results. They are listed below, including both the less and more important ones. First, the generalization of von Kármán [3, 4] work to other similar configurations, see Figs. 2, where only Figs. 2(d), 2(f) have been addressed in his work. The two vortex configurations proposed by Crow [6] and Jiménez [7] are only valid for some range of parameters, due to the cutoff approach. This fact is brought in this paper, showing which regions are valid and why, in order to avoid unrealistic results. The same is done for the Rennich and Lele [9] four vortex configuration, also studied by Fabre and Jacquin [10], who limit themselves to one particular configuration, while this time the circulation ratio and the cutoff length are studied in

a wide range. Their way to employ the cutoff is different to that employed in this article. They developed a more elegant relation between cutoff and vortex radius, that allows them to study short wavelengths, but they had to chose the same vortex model one for all. On the contrary, the approach followed here permits to convert the filament results based on cutoff length to any vortex model. The previous are some of the new outcomes of the work, regarding the vortex filaments approach, however, the comparisons with viscous analysis are also new. In the two counter-rotating vortices case, some previous works exists: Benton and Bons [69] and Brion et al. [70], but they address the problem from a different approach and do not specify as many details of the comparison, because they pursue different aims. For the four vortex configuration, it is the first known case to the authors where a quantitative comparison is given between the two analogies, and therefore, this is one of the most valuable results obtained in the present work. The last outcome of that being a very good agreement between both analogies in this context, which will help the community to apply filament vortex stability analysis as a faster substitute for global stability in more situations. Once the novelties of the present research are exposed clearly, it is time to highlight that the main goal of it is the presentation of a comprehensive evaluation of the method, collecting a wide range of studies under a single methodology, which can be use for many more configurations.

Apart from the earlier, a general outcome of the work, particularly from the relevance for the aeronautical community, is the fact that this simple and reliable approach, could be used as a general methodology to solve a really wide variety of vortical configurations that can represent the aircraft wake. Being more specific, this methodology has permitted to achieve results as the Kelvin-Helmholtz instability, the von Kármán vortex street, the Crow instability, and the inner vortex instability for systems of four vortices, all these analyzed here. It is generally observed that the vortex core shape is irrelevant for all these if the vortices are far apart, and it becomes important (as it should be) when the size of the vortices becomes comparable to their separation.

Although it escapes from the scope of the work, it is provided a little insight into the idea of how the present results could help to destroy the aircraft wake, which is the final goal towards all this and other investigations are directed. An starting point for control strategies to destroy the vortex wake could be to select the highest amplification rate wavenumber for a particular configuration. Done so, this mode could be excited, but as the modes found here do not have frequency, the excitation has to be done in space, rather than in time. Still, given that the aircraft is moving at a particular speed, an appropriate excitation in time will provide a spatial excitation, which should match the maximum amplification rate wavelength. Doing so, specifically if the shape of the perturbation matches the shape of the mode, it could be excited earlier, and therefore the wake would be destroyed faster. However, the four vortex case show a particular case where the most unstable mode, only affect the inner vortices, so the excitation of this mode, will only destroy these vortices, remaining still a two vortex wake. Nevertheless, the destruction process involves many other non-linear mechanisms, which could most probably also be excited to achieve this in a more effective manner. The interaction between the actual actuator for the wake destabilization and the aircraft performance should be evaluated to avoid undesired behaviors. However, as the lift of the plane is a function of the vortices circulation, as long as it is not modified, the effect on the aircraft performance should be little.

From a physical point of view, a shortcoming of both approaches is the treatment of the axial flow direction as homogeneous, neglecting a viscous diffusion that is a function of this spatial coordinate. This issue will be treated in future work.

Acknowledgements

Support of the Marie Curie Grant PIRSES-GA-2009-247651 “FP7-PEOPLE-IRSES: ICOMASEF - Instability and Control of Massively Separated Flows” as well as from the Plan Nacional Grants TRA2009-13648 “Metodologías Computacionales para la Predicción de Inestabilidades Globales Hidrodinámicas y Aeroacústicas en Flujos Complejos” and TRA2012-34148 “Mejoras del Rendimiento Aerodinámico de Alas Mediante Control de Mecanismos de Inestabilidad Global” are gratefully acknowledged. Discussions with Dr. J. D. Crouch regarding comparisons of viscous and inviscid results as well as the assistance of Dr. P. Paredes with the use of the BiGlobal methodology are gratefully acknowledged. The authors would like to thank the anonymous reviewers for their thorough review and highly appreciate the constructive and valuable comments and suggestions, which significantly contributed to improve the quality of the publication.

Appendix A. Formulas used in section 2.1.3

A list of formulas used in section 2.1.3 is provided in this appendix:

$$
\begin{aligned}
f_1(\varphi) &= \sum_{q=1}^{\infty} \frac{1-\cos(q\varphi)}{q^2} \\
f_2(\varphi) &= \sum_{q=1}^{\infty} (-1)^q \frac{1-\cos(q\varphi)}{q^2} \\
f_3(l/e) &= 1 + 2\sum_{q=1}^{\infty} \frac{1}{(ql/e)^2+1} \\
f_4(l/e) &= \sum_{q=1}^{\infty} \frac{(ql/e)^2-1}{[(ql/e)^2+1]^2} \\
f_5(\varphi, l/e) &= \sum_{q=1}^{\infty} \frac{(ql/e)^2-1}{[(ql/e)^2+1]^2} \cos(q\varphi) \\
f_6(\varphi, l/e) &= \sum_{q=1}^{\infty} \frac{q\sin(q\varphi)}{[(ql/e)^2+1]^2} \\
f_7(l/e) &= \sum_{q=1}^{\infty} \frac{1}{[(q-1/2)l/e]^2+1} \\
f_8(l/e) &= \sum_{q=1}^{\infty} \frac{[(q-1/2)l/e]^2-1}{[((q-1/2)l/e)^2+1]^2} \\
f_9(\varphi, l/e) &= \sum_{q=1}^{\infty} \frac{[(q-1/2)l/e]^2-1}{[((q-1/2)l/e)^2+1]^2} \cos[(q-1/2)\varphi] \\
f_{10}(\varphi, l/e) &= \sum_{q=1}^{\infty} \frac{(q-1/2)\sin[(q-1/2)\varphi]}{[((q-1/2)l/e)^2+1]^2} \\
A_1(\varphi, l/e) &= f_1(\varphi) + (l/e)^2[1/2 - f_4(l/e)] \\
B_1(\varphi, l/e) &= 2\mathrm{i}(l/e)^3 f_6(\varphi, l/e) \\
C_1(\varphi, l/e) &= (l/e)^2[1/2 - f_5(\varphi, l/e)] \\
A_2(\varphi, l/e) &= f_1(\varphi) - (l/e)^2 f_8(l/e) \\
B_2(\varphi, l/e) &= 2\mathrm{i}(l/e)^3 f_{10}(\varphi, l/e) \\
C_2(\varphi, l/e) &= -(l/e)^2 f_9(\varphi, l/e)
\end{aligned}
\tag{A.1}
$$

References

[1] P. R. Spalart, Airplane trailing vortices, Ann. Rev. of Fluid Mechanics 30 (1998) 107–138.
[2] A. Broderick, P. Bevilaqua, J. Crouch, F. Gregory, F. Hussain, B. Jeffers, D. Newton, D. Nguyen, J. Powell, A. Spain, R. Strone, K. Willcox, Wake Turbulence - An Obstacle to Increased Air Traffic Capacity, National Research Council, 2008.
[3] T. von Kármán, Über den mechanismus des widerstandes, den ein bewegter körper in einer flüssigkeit erfährt, Nachr. Ges. Wissenschaft. Göttingen (1911) 509–517, (in German).
[4] T. von Kármán, Über den mechanismus des widerstandes, den ein bewegter körper in einer flüssigkeit erfährt, Nachr. Ges. Wissenschaft. Göttingen (1911) 547–556, (in German).
[5] C. d. Donaldson, A. J. Bilanin, Vortex Wakes of Conventional Aircraft, Tech. Rep., AGARD, TR AG-204, 1975.
[6] S. C. Crow, Stability Theory for a Pair of Trailing Vortices, AIAA J. 8 (1970) 2172–2179.
[7] J. Jiménez, Stability of a pair of co-rotating vortices, Phys. Fluids 18 (11) (1975) 1580–1581.
[8] J. D. Crouch, Instability and Transient Growth for Two Trailing-Vortex Pairs, J. Fluid Mech. 350 (1997) 311–330.

[9] S. C. Rennich, S. K. Lele, Method for Accelerating the Destruction of Aircraft Wake Vortices, Journal of Aircraft 36 (2) (1999) 398–404.
[10] D. Fabre, L. Jacquin, Stability of a four-vortex aircraft wake model, Phys. Fluids 12 (10) (2000) 2438–2443.
[11] W. T. Kelvin, Floating magnets (illustrating vortex-systems), Nature (London) 18 (1878) 13–14.
[12] J. J. Thomson, On the Motion of Vortex Rings, Macmillan, London (1883) 94–108.
[13] T. H. Havelock, The stability of motion of rectilinear vortices in ring formation, Philos. Mag. 11 (1931) 617.
[14] L. J. Campbell, Transverse normal modes of finite vortex arrays, Physical Review A 24 (1) (1981) 514–534.
[15] L. G. Kurakin, V. I. Yudovich, The stability of stationary rotation of a regular vortex polygon, Chaos 12 (3) (2002) 574–595.
[16] N. E. Joukowski, Vortex theory of a rowing screw, Trudy Otdeleniya Fizicheskikh Nauk Obshchestva Lubitelei Estestvoznaniya 16 (1) (1912) 31, (in Russian).
[17] H. Aref, Motion of three vortices, Phys. Fluids 22 (3) (1979) 393–400.
[18] H. Aref, Stability of relative equilibria of three vortices, Phys. Fluids 21 (9) (2009) 4101–1–22.
[19] H. Aref, Point vortex motions with a center of symmetry, Phys. Fluids 25 (12) (1982) 2183–2187.
[20] W. T. Kelvin, Vibrations of a columnar vortex, Phil. Mag. 10 (1880) 155–168.
[21] H. Levy, A. G. Forsdyke, The steady motion and stability of a helical vortex, Proc. R. Soc. Lond. A 120 (1928) 670–690.
[22] R. L. Ricca, The effect of torsion on the motion of a helical vortex filament, J. Fluid Mech. 273 (1994) 241–259.
[23] P. A. Kuibin, V. L. Okulov, Self-induced motion and asymptotic expansion of the velocity field in the vicinity of a helical vortex filament, Phys. Fluids 10 (3) (1998) 607–614.
[24] V. L. Okulov, On the stability of multiple helical vortices, J. Fluid Mech. 521 (2004) 319–342.
[25] V. L. Okulov, J. N. Sørensen, Instability of the far wake behind a wind turbine, Abs. 21th ICTAM-2004, Warsaw, Poland .
[26] M. Lessen, F. Paillet, The stability of a trailing line vortex. Part 2. Viscous theory, J. Fluid Mech. 65 (1974) 769–779.
[27] M. R. Khorrami, M. R. Malik, R. L. Ash, Application of spectral collocation techniques to the stability of swirling flows, J. Comp. Phys. 81 (1) (1989) 206–229.
[28] M. R. Khorrami, On the viscous modes of instability of a trailing line vortex, J. Fluid Mech. 225 (1991) 197–212.
[29] M. Khorrami, Behavior of asymmetric unstable modes of a trailing line vortex near the upper neutral curve, Phys. Fluids 4 (6) (1992) 1310–1313.
[30] E. W. Mayer, K. G. Powell, Viscous and inviscid instabilities of a trailing vortex, J. Fluid Mech. 245 (1992) 94–114.
[31] V. Theofilis, Advances in Global Linear Instability Analysis of Nonparallel and Three-Dimensional Flows, Prog. in Aero. Sciences 39 (4) (2003) 249–315.
[32] V. Theofilis, Global linear instability, Ann. Rev. of Fluid Mechanics 43 (2011) 319–352.
[33] F. Gómez, S. Le Clainche, P. Paredes, M. Hermanns, V. Theofilis, Four decades of studying global linear instability: Problems and challenges, AIAA Journal 50 (12) (2012) 2731–2743.
[34] D. Sipp, L. Jacquin, Widnall instabilities in vortex pairs, Phys. Fluids 15 (7) (2003) 1861–1874.
[35] S. Hein, V. Theofilis, On instability characteristics of isolated vortices and models of trailing-vortex systems, Comp. and Fluids 33 (5-6) (2004) 741–753.
[36] L. Jacquin, D. Fabre, D. Sipp, V. Theofilis, H. Vollmers, Instability and unsteadiness of aircraft wake vortices, Aero. Sci. Tech. 7 (8) (2003) 577–593.
[37] L. M. González, V. Theofilis, R. Gómez-Blanco, Finite element methods for viscous incompressible BiGlobal instability analysis on unstructured meshes, AIAA Journal 45 (4) (2007) 840–854.
[38] L. M. Gonzalez, R. Gomez-Blanco, V. Theofilis, Eigenmodes of a Counter-Rotating Vortex Dipole, AIAA Journal 46 (11) (2008) 2796–2805.
[39] M. S. Broadhurst, V. Theofilis, S. J. Sherwin, Spectral element stability analysis of vortical flows, in: R. Govindarajan (Ed.), Sixth IUTAM Symposium on Laminar-Turbulent Transition, vol. 78 of *Fluid Mec. A.*, 153–158, 2006.
[40] P. Paredes, V. Theofilis, D. Rodríguez, J. A. Tendero, The PSE-3D instability analysis methodology for flows depending strongly on two and weakly on the third spatial dimension, in: 6th AIAA Theoretical Fluid Mechanics Conference, Honolulu, HI, USA, June 27-30, vol. 2011-3752, 1–21, 2011.
[41] M. Abid, M. E. Brachet, Direct numerical simulations of the Batchelor trailing vortex by a spectral method, Phys. Fluids 10 (2) (1998) 469–475.
[42] F. Laporte, A. Corjon, Direct numerical simulations of the elliptic instability of a vortex pair, Phys. Fluids 12 (5) (2000) 1016–1031.
[43] R. L. Bristol, J. M. Ortega, P. S. Marcus, O. Savas, On cooperative instabilities of parallel vortex pairs, J. Fluid Mech. 517 (2004) 331–358.
[44] L. Nybelen, R. Paoli, Direct and Large-Eddy Simulations of Merging in Corotating Vortex System, AIAA Journal 47 (1) (2009) 157–167.
[45] P. Billant, P. Brancher, J. M. Chomaz, Three-dimensional stability of a vortex pair, Phys. Fluids 11 (8) (1999) 2069–2077.
[46] G. Winckelmans, R. Cocle, L. Dufresne, R. Capart, Vortex methods and their application to trailing wake vortex simulations, Academie des Sciences. Comptes Rendus, Physique 6 (2005) 467–86.
[47] P. Chatelain, A. Curioni, M. Bergdorf, D. Rossinelli, W. Andreoni, P. Koumoutsakos, Billion vortex particle direct numerical simulations of aircraft wakes, Comput. Method. Appl. M. 197 (13-16) (2008) 1296–1304.
[48] P. Chatelain, M. Gazzola, S. Kern, P. Koumoutsakos, Optimization of Aircraft Wake Alleviation Schemes through an Evolution Strategy, in: J. M. L. Palma, M. Dayde, O. Marques, J. C. Lopez (Eds.), High Performance Computing for Computational Science - VECPAR 2010, vol. 6449 of *Lect. Notes Comput. Sc.*, 210–221, 2011.
[49] J. H. Walther, M. Guenot, E. Machefaux, J. T. Rasmussen, P. Chatelain, V. L. Okulov, J. N. Sørensen, M. Bergdorf, P. Koumoutsakos, A numerical study of the stabilitiy of helical vortices using vortex methods - art. no. 012034, in: M. O. L. Hansen, K. S. Hansen (Eds.), Science of Making Torque from Wind, vol. 75 of *J. Phys. Conf. Ser.*, 12034, 2007.
[50] T. Leweke, C. H. K. Williamson, Cooperative elliptic instability of a vortex pair, J. Fluid Mech. 360 (1998) 85–119.
[51] F. Laporte, T. Leweke, Elliptic instability of counter-rotating vortices: Experiment and direct numerical simulation, AIAA Journal 40 (12) (2002) 2483–2494.
[52] C. H. K. Williamson, Vortex dynamics in the cylinder wake, Ann. Rev. of Fluid Mechanics 28 (1996) 477–539.
[53] F. R. Hama, Progressive deformation of a curved vortex filament by its own induction, Phys. Fluids 5 (10) (1962) 1156–1162.

[54] R. J. Arms, F. R. Hama, Localized-induction concept on a curved vortex and motion of an elliptic vortex ring, Phys. Fluids 8 (4) (1965) 553–559.
[55] S. E. Widnall, D. B. Bliss, A. Zalay, Aircraft Wake Turbulence and its Detection, in: J. H. Olsen, A. Goldburg, M. Rogers (Eds.), Aircraft Wake Turbulence and Its Detection, Plenum, New York, 305–338, 1971.
[56] D. W. Moore, P. G. Saffman, Motion of a vortex filament with axial-flow, Phil. Trans. R. Soc. A 272 (1226) (1972) 403–429.
[57] S. E. Widnall, Structure and dynamics of vortex filaments, Ann. Rev. of Fluid Mechanics 7 (1975) 141–165.
[58] A. J. Callegari, L. Ting, Motion of a curved vortex filament with decaying vortical core and axial velocity, SIAM J. Appl. Math. 35 (1) (1978) 148–175.
[59] Y. Fukumoto, T. Miyazaki, Three-dimensional distortions of a vortex filament with axial velocity, J. Fluid Mech. 222 (1991) 369–416.
[60] R. Klein, A. J. Majda, Self-stretching of a perturbed vortex filament I. The asymptotic equation for deviations from a straight line, Physica D 49 (1991) 323–352.
[61] A. Segalini, P. H. Alfredsson, A simplified vortex model of propeller and wind-turbine wakes, J. Fluid Mech. 725 (2013) 91–116.
[62] C.-Y. Tsai, S. E. Widnall, The stability of short waves on a straight vortex filament in a weak externally imposed strain field, J. Fluid Mech. 73 (1976) 721–733.
[63] G. K. Batchelor, An Introduction to Fluid Dynamics, Cambridge University Press, 1967.
[64] D. Fabre, L. Jacquin, A. Loof, Optimal perturbations in a four-vortex aircraft wake in counter-rotating configuration, J. Fluid Mech. 451 (2002) 319–328.
[65] M. Abramowitz, I. A. Stegun, Handbook of Mathematical Functions with Formulas, Graphs, and Mathematical Tables, chap. 6.3 psi (Digamma) Function., New York: Dover, 258–259, 1972.
[66] P. Paredes, M. Hermanns, S. Le Clainche, V. Theofilis, Order 10(4) speedup in global linear instability analysis using matrix formation, Comput. Method. Appl. M. 253 (2013) 287–304.
[67] J. A. Tendero, P. Paredes, M. Roura, R. Govindarajan, V. Theofilis, BiGlobal and Point Vortex Methods for the Instability Analysis of Wakes, in: 43rd AIAA Fluid Dynamics Conference and Exhibit, San Diego, CA, USA, June 24-27, vol. 2013-2820, 1–16, 2013.
[68] J. A. Tendero, P. Paredes, M. Roura, R. Govindarajan, V. Theofilis, Filament Vortex and Global Instability Analysis of the Crow Mode, in: V. Theofilis, J. Soria (Eds.), Fluid Mechanics and its Applications series, International Conference on Instability and Control of Massively Separated Flows, Prato, Italy, Sept. 4-6, (accepted), 2013.
[69] S. I. Benton, J. P. Bons, Three-dimensional Instabilities in Vortex/Wall Interactions: Linear Stability and Flow Control, in: 52nd AIAA Aerospace Sciences Meeting, 13-17 Jan., National Harbor, MD, USA, vol. 2014-1267, 1–15, 2014.
[70] V. Brion, D. Sipp, L. Jacquin, Optimal amplification of the Crow instability, Phys. Fluids 19 (11) (2007) 111703–1–4.